ChemBioChem

Combining Chemistry and Biology

Chemistry Europe

European Chemical Societies Publishing

Accepted Article

Title: Synthesis, Photophysical Properties and Biological Evaluation of New Conjugates BODIPY – Dinuclear Trithiolato-Bridged Ruthenium(II)-Arene Complexes

Authors: Oksana Desiatkina, Ghalia Boubaker, Nicoleta Anghel, Yosra Amdouni, Andrew Hemphill, Julien Furrer, and Emilia Paunescu

To be cited as: *ChemBioChem* **2022**, e202200536

Link to VoR: https://doi.org/10.1002/cbic.202200536

WILEY-VCH

Synthesis, Photophysical Properties and Biological Evaluation of New Conjugates BODIPY – Dinuclear Trithiolato-Bridged Ruthenium(II)-Arene Complexes

Oksana Desiatkina[a], Ghalia Boubaker[b], Nicoleta Anghel[b], Yosra Amdouni[b,c], Andrew Hemphill[b,]*, Julien Furrer[a,]*, Emilia Păunescu[a,]*

[a]Department of Chemistry, Biochemistry and Pharmaceutical Sciences, University of Bern, Freiestrasse 3, CH-3012 Bern, Switzerland.
[b]Institute of Parasitology, Vetsuisse Faculty, University of Bern, Länggassstrasse 122, CH-3012 Bern, Switzerland.
[c]Laboratoire de Parasitologie, Université de la Manouba, Institution de la Recherche et de l'Enseignement Supérieur Agricoles, École Nationale de Médecine Vétérinaire de Sidi Thabet, Sidi Thabet 2020, Tunisia.

Abstract

The synthesis, photophysical properties and antiparasitic efficacy against *Toxoplasma gondii* β-gal (RH strain tachyzoites expressing β-galactosidase) grown in human foreskin fibroblast monolayers (HFF) of a series of 15 new conjugates BODIPY-trithiolato-bridged dinuclear ruthenium(II)-arene complexes are reported (BODIPY = 4,4-difluoro-4-bora-3a,4a-diaza-*s*-indacene, derivatives used as fluorescent markers). The influence of the bond type (amide *vs* ester), as well as that of the length and nature (alkyl *vs* aryl) of the spacer between the dye and the diruthenium(II) complex moiety, upon the fluorescence and the biological activity were evaluated. The assessed photophysical properties revealed that despite an important fluorescence quenching effect observed after conjugating the BODIPY to the diruthenium unit, the hybrids could nevertheless be used as fluorescent tracers.

Although the antiparasitic activity of these series of conjugates appears limited, the compounds demonstrate potential as fluorescent probes to be used for investigating the intracellular trafficking of trithiolato-bridged dinuclear Ru(II)-arene complexes *in vitro*.

Keywords: Antiparasitic activity, antiprotozoal agents, BODIPY, fluorescence, photophysical properties, *Toxoplasma gondii*, Trithiolato dinuclear ruthenium(II)-arene complexes.

1. Introduction

The study of ruthenium complexes for therapeutical purposes is an active area of research for more than two decades.[1] Developed initially as a potential alternative to platinum based anticancer drugs,[2] ruthenium(II)-arene complexes were also considered for other pharmacological properties, notably as antiparasitic,[3] and antibacterial compounds.[4]

Cationic trithiolato-bridged dinuclear ruthenium(II)-arene complexes (general formula for symmetric $[(\eta^6\text{-arene})_2Ru_2(\mu_2\text{-}SR)_3]^+$, and mixed $[(\eta^6\text{-arene})_2Ru_2(\mu_2\text{-}SR^1)_2(\mu_2\text{-}SR^2)]^+$ complexes) are highly cytotoxic against human cancer cells (low micromolar range IC_{50} values (half maximal inhibitory concentration))[5] and present interesting antiparasitic efficacy against *Toxoplasma gondii*,[6] *Neospora caninum*[7] and *Trypanosoma brucei*.[8] Yet little is known about the traffic and fate of these complexes in cells and how it relates to their anticancer or antiparasitic effect. Transmission Electron Microscopy (TEM) of *T. gondii* treated with various trithiolato-bridged dinuclear ruthenium(II)-arene compounds had identified the parasites mitochondrion as a potential target.[6] Nonetheless, a better understanding of their mechanism of action and the identification of specific biological targets would allow to design and develop more efficient compounds.

ICP-MS[9] (inductively coupled plasma mass spectrometry) or fluorescence microscopy[10] of complexes that are fluorescent *per se* or that are tagged with fluorescent dyes can be used as support for the identification of the cellular localization of metal-based bioactive compounds. The development of traceable therapeutic agents as fluorophore-labelled conjugates of metal-based drugs is a promising approach.[11] For example, in the quest of compounds presenting both therapeutic and imaging properties, the Ru(II)-arene moiety was coupled to numerous organic fluorophores including anthracene,[12] pyrene,[13] naphthalimide,[14] coumarins,[15] rhodamine,[16] BODIPYs,[11c] or porphyrins.[17] However, some of these conjugates were not suitable for bioimaging purposes, mostly due to emission quenching after coupling the metal unit to the fluorophore (e.g., through a photoinduced electron transfer (PET) or by de-excitation of the triplet excited state[15b]) was too important.

From the large library of fluorescent dyes, BODIPYs (boron dipyrromethene, 4,4-difluoro-4-bora-3*a*,4*a*-diaza-*s*-indacene) remain among the most attractive. They are chemically inert (stable in physiological pH-range, only decomposing in strong acidic and basic conditions[18]), and well soluble in common organic solvents with photophysical properties mostly independent of solvent polarity. BODIPYs display high photostability, small Stokes shifts, high fluorescence quantum yields, neutral charge, and sharp absorption and emission bands,[19] while their properties can be tuned *via* chemical modifications.[20] Since BODIPY derivatives are also non-toxic,[21] they are especially useful for cell imaging studies and as biological probes.[19a, 22] Although BODIPY derivatives exhibit reduced activity in cellular experiments, anchoring this fluorophore to an organometallic moiety could not only significantly modify the physicochemical properties of the metal complex and change their intracellular localization, but also alter the mode of action of the conjugates. For instance, platinum-fluorophore

complexes were not localized in the cellular nucleus,[23] and some platinum complexes bearing BODIPYs exhibited preferential mitochondrial distribution.[24]

Numerous examples of biologically active metal-based compounds tethered with BODIPY dyes have been reported.[10, 25] Various platinum,[11a, 24b] ruthenium,[11c] osmium,[11c] iridium,[26] gold,[27] titanium,[28] and copper,[29] complexes with BODIPY appendices at the level of the ligands were identified as potential bioactive traceable fluorescent probes, some examples being summarized in Figure 1.

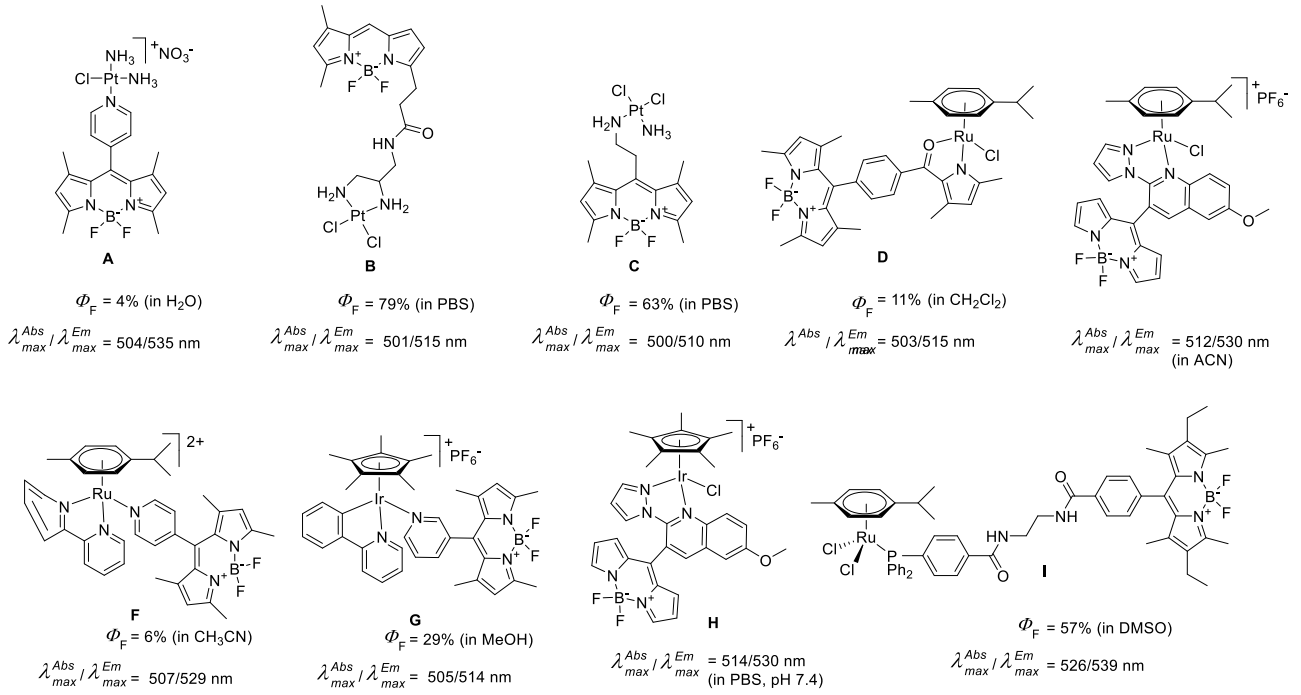

Figure 1. Structure and physico-chemical properties of reported metal-complex - BODIPY conjugates.

For the BODIPY-labelled platinum compound **A**[30] (Figure 1), highly antiproliferative against cancer cells, the complexation to the metal led to fluorescence quantum yield decrease, which was ascribed to the oxidative photoinduced electron transfer (PET) from the excited core of BODIPY to the pyridyl group.[31] Using confocal laser scanning microscopy, **A** showed a distinct mitochondrial distribution in cancer cells and its fluorescence intensity was higher than that of the ligand, paralleling the enhanced cellular uptake of the complex *vs* the free ligand.

Derivatives like **B**[11a, 24a] and **C**[24a] exhibited cytotoxic and DNA-damaging properties, along with robust *in vivo* fluorescence. For **B** microscopy revealed a predominately cytosolic/perinuclear localization, with nuclear distribution at higher concentrations,[11a] while **C** localized in the cytoplasm near the nucleus.[24a]

The nature of the ligand and that of the coordinated metal center can strongly influence the photophysical properties of the conjugates. Half-sandwich Ru(II) complex **D**[32] (Figure 1) was highly fluorescent, photostable while exhibiting negligible cytotoxicity at concentrations used for imaging purposes. Live cell imaging investigations revealed that **D** localized specifically in the mitochondria, and coordination to the metal center led to fluorescence quenching.

Other properties of the BODIPY fluorophores, as the generation of singlet oxygen on light activation for photodynamic therapy/photocytotoxicity, were exploited.[11b, 24b, 24c, 33] For example, BODIPY-functionalized Ru(II)-arene complex **E**[11d] (Figure 1) behaved as a potential 'theranostic' agent, accumulating in the cancer cells lysosome, exhibiting high photo-cytotoxicity under visible light on cancer cells, while being less toxic in the dark. Similarly, dyad **F** (Figure 1) was shown to effectively enable cancer cells photo-inactivation,[25a, 34] the coordination of the Ru(II)-arene unit being followed by an important fluorescence quenching.[25a] A partial quenching was noticed for **F** upon the complexation of the organometallic entity, an effect explained by intramolecular PET.[25a, 34]

For the half-sandwich iridium(III) complex **G**[35] (Figure 1), the introduction of the pyridyl-BODIPY ligand increased the lipophilicity and the cytotoxicity. Living cell fluorescence imaging indicated both **G** and its free ligand were membrane permeant and accumulated in cells,[35] being detected indistinctly as large diffuse zones and small bright spots in the cytoplasm, the amount of the dyad being higher compared to that of the ligand.

Complex **H**[36] exhibited medium cytotoxicity towards cancer cells, with a strong influence of the BODIPY on the cellular uptake and preferred cell membranes accumulation without reaching the nuclei. The BODIPY–phosphane ligand in **I**[11c] (Figure 1) led to 'theranostics' featuring Ru(II), Os(II) and Au(I). In **I** the fluorescence was moderately quenched, attributed to the fact that the compound is prone to PET,[37] and can promote BODIPY phosphorescence.[38] The *in vitro* imaging showed that **I** and the BODIPY-phosphane ligand rapidly bind to the biological membranes, with no clear specificity, the uptake and distribution properties of **I** being determined by the BODIPY moiety.

Previous studies have shown that trithiolato-bridged diruthenium complexes are highly stable constituting good substrates for derivatization using the 'chemistry on the complex' strategy. Conjugates can be obtained by anchoring molecules of interest on the bridge thiols, and hybrids with peptides,[39] the anticancer drug chlorambucil,[40] coumarin fluorophores,[41] antimicrobial drugs[42] and nucleobases[43] were recently synthesized and assessed for their anticancer or antiparasitic properties. Interestingly, trithiolato-bridged diruthenium conjugates tagged with coumarin fluorophores showed promising anti-*Toxoplasma* properties, but also completely quenched fluorescence.[41] Alternatively, BODIPY analogues have been used for the study of lipid metabolism in *T. gondii*.[44]

The current study was focused on the obtainment of new conjugates BODIPY-trithiolato-bridged diruthenium(II)-arene units as potential antiparasitic and intracellular fluorescent tracking agents. To have a better input on the parameters that can influence the photophysical properties and/or the cytotoxicity/antiparasitic activity of the dyads, different structural elements were varied as: (i) the type of the bond connecting the two entities (ester *vs* amide), (ii) the length of the spacer, and iii) the nature of the BODIPY dye (with an *meso*-aliphatic or an aromatic substituent).

The photophysical properties of the new conjugates as well as those of the corresponding free dyes were studied. The antiparasitic activity of the compounds was assessed against the apicomplexan parasite

T. gondii β-gal and the cytotoxicity of the compounds was determined on HFF. Representative derivatives were also submitted to TEM (Transmission Electron Microscopy) and fluorescence microscopy studies to gain more insight on the compounds' potential targets and intracellular localization.

2. Results and Discussion

2.1. Chemistry

Three mix trithiolato diruthenium(II)-arene derivatives bearing hydroxy **2**, amino **3** and carboxy **4** groups on one of the bridging thiols were synthesized following a two-step reported procedure[41, 45] (Scheme 1), using the ruthenium dimer $[Ru(\eta^6\text{-}p\text{-}MeC_6H_4Pr^i)Cl]_2Cl_2$[46] and 4-*tert*-butylbenzenemethanethiol for the first step, and the resulted dithiolato intermediate **1** and 4-mercaptophenol, 4-aminobenzenethiol and 2-(4-mercaptophenyl)acetic acid for the second step.

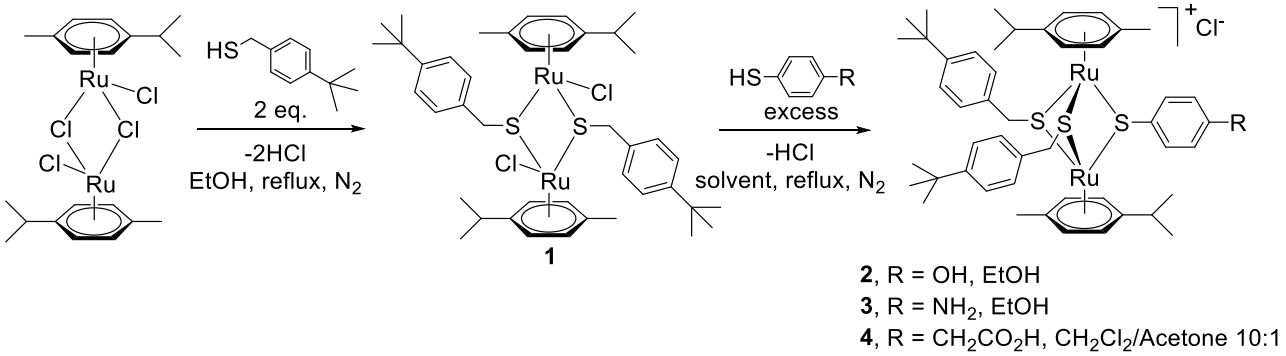

Scheme 1. Synthesis of the dinuclear dithiolato **1** and OH, NH_2, CH_2CO_2H functionalized trithiolato ruthenium(II)-arene complexes **2**, **3** and **4**.

The synthetic approaches to obtain the borondipyrromethene core are based on the porphyrin chemistry research.[47] A first library of carboxy-functionalized *meso*-BODIPY compounds **9**-**12** with aliphatic chains of various length between the fluorophore and the CO_2H group was synthesized by adapting reported protocols.[48] The BODIPYs were obtained by the condensation of 3-ethyl-2,4-dimethylpyrrole with four commercially available acid chlorides as acylium equivalent: methyl 4-chloro-4-oxobutyrate, methyl 6-chloro-6-oxohexanoate, methyl 8-chloro-8-oxooctanoate and methyl 10-chloro-10-oxodecanoate (Scheme 2).[48a] The acylpyrrole intermediates (not isolated) were reacted DIPEA (*N*,*N*-diisopropylethylamine) and $BF_3{\cdot}OEt_2$ (boron trifluoride etherate) to afford the methyl protected carboxy BODIPY dyes **5**-**8** (yields 32-52%). In a second step, the esters **5**-**8** were hydrolyzed in basic conditions (KOH)[48b-d] leading to the isolation of the BODIPY carboxy analogues **9**-**12** in medium yields (45%-quantitative, Scheme 2).

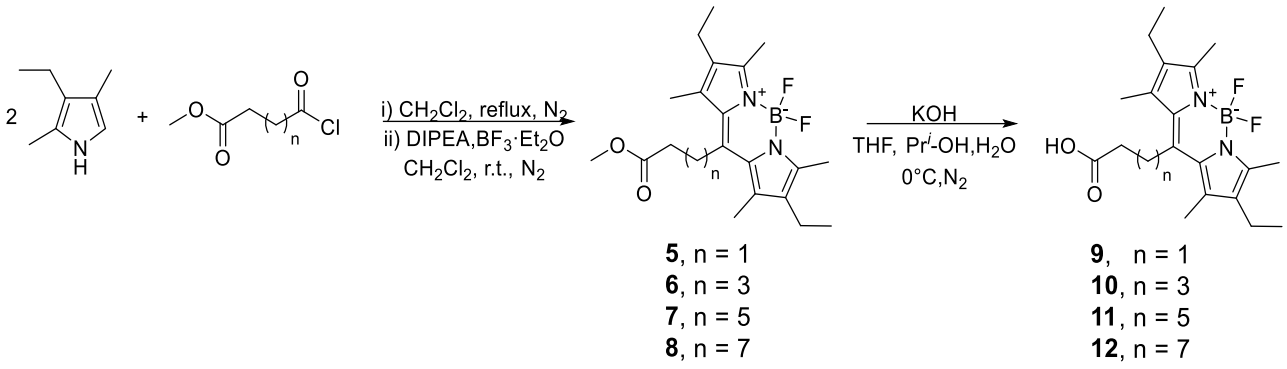

Scheme 2. Synthesis of the carboxy-BODIPY dyes **9**-**12**.

To assess the influence of the functional group present on the fluorophore on the photophysical properties of the BODIPY-trithiolato-diruthenium conjugates, one hydroxy (**14**) and two amino-functionalized (**17** and **18**) *meso*-substituted BODIPY compounds with short alkyl spacers were synthesized following the reaction sequence presented in Scheme 3. **14** was obtained in two steps using reported protocols[48a] (Scheme 3 (top)). First, the acetyl protected intermediate **13** was synthesized by the reaction of 3-ethyl-2,4-dimethylpyrrole with 2-chloro-2-oxoethyl acetate (commercially available) as acylium equivalent. Addition of DIPEA to the intermediate acylpyrrole formed *in situ*, followed by application of BF_3·OEt_2 afforded the BODIPY dye **13** (35%). Ester hydrolysis in basic conditions (LiOH) released the hydroxy BODIPY **14**, isolated in 43% yield. **17** and **18** were obtained following the reaction pathway presented in Scheme 3 (bottom) using previously described procedures.[49] First, 3-ethyl-2,4-dimethylpyrrole was reacted with phthalimide protected derivatives 1,3-dioxo-2-isoindolineacetyl chloride and 1,3-dioxo-2-isoindolinebutanoyl chloride as acylium equivalents, affording intermediates **15** and **16** isolated with 44 and 26% yield, respectively. In a second step, compounds **15** and **16** were deprotected using hydrazine in refluxing EtOH,[49a] and the BODIPY amino alkyl derivatives **17** and **18** were isolated in 25 and 18% yield.

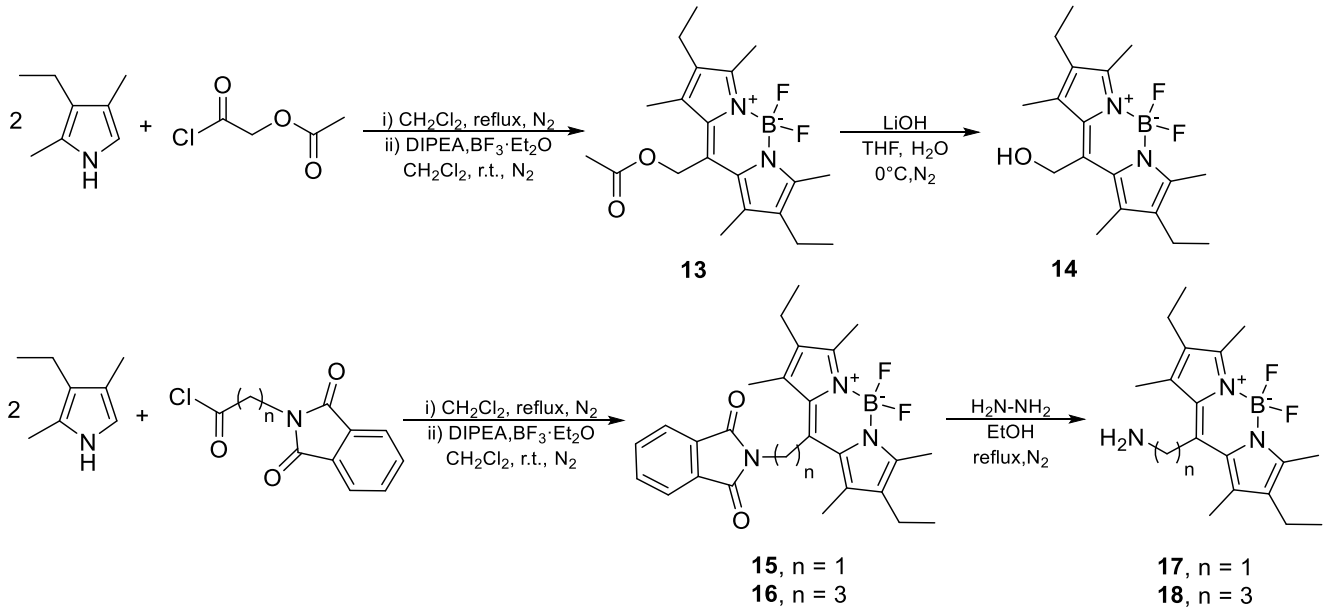

Scheme 3. Synthesis of the BODIPY dyes containing a hydroxy group **14** (top) and an amino group **17** and **18** (bottom).

The carboxy BODIPYs **9**-**12** were reacted with the diruthenium hydroxy and amine derivatives **2** and **3** affording the ester **19**-**22**, and respectively, amide dyads **23**-**26** (Scheme 4).

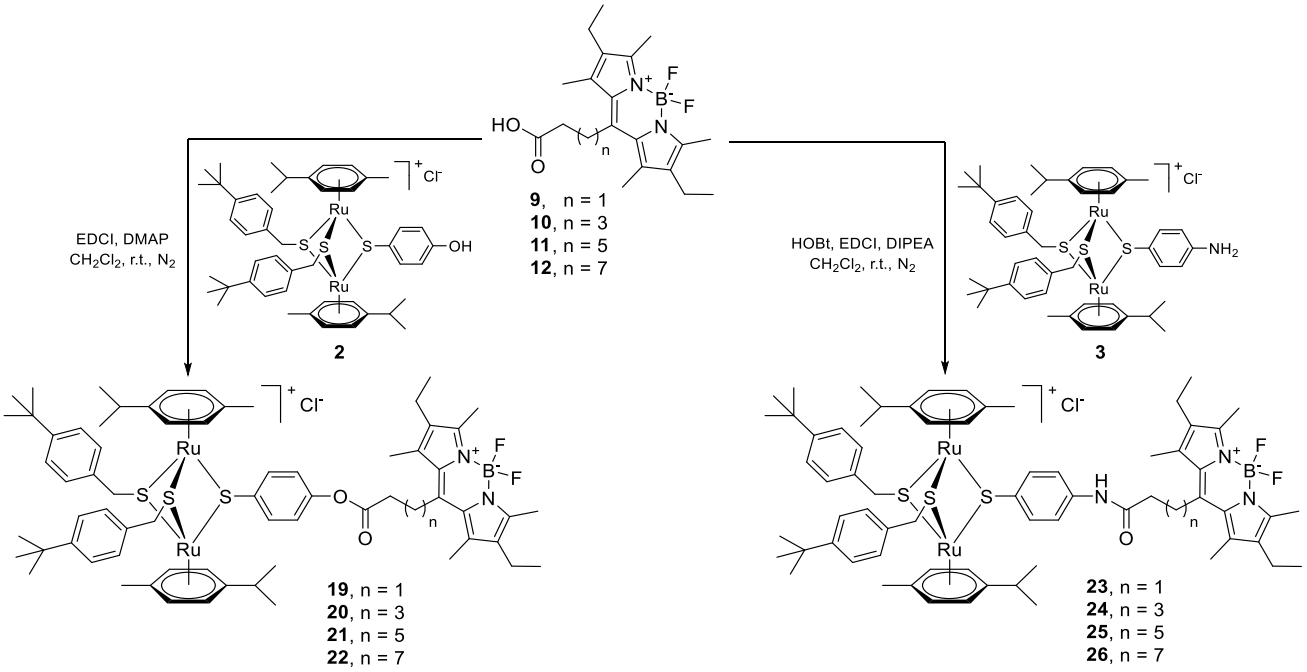

Scheme 4. Synthesis of the ester **19**-**22** (left) and amide **23**-**26** (right) conjugates BODIPY-dinuclear trithiolato ruthenium(II)-arene complexes containing alkyl spacers of various lengths.

For the esters conjugates, EDCI (*N*-(3-dimethylaminopropyl)-*N*′-ethylcarbodiimide hydrochloride) was used as coupling agent and DMAP (*N*,*N*-dimethylpyridin-4-amine) as base[50] and **19**-**22** were isolated in 12-93% yield. For the amide analogues, the reactions were realized in the presence of EDCI and HOBt (1-hydroxybenzotriazole) as coupling agents and of DIPEA as basic catalyst,[51] conjugates **23**-**26** being isolated in 22-74% yield.

The BODIPY hydroxy **14** and the amino **17** and **18** derivatives were reacted with carboxy diruthenium complex **4**, using the reaction conditions presented in Scheme 5.

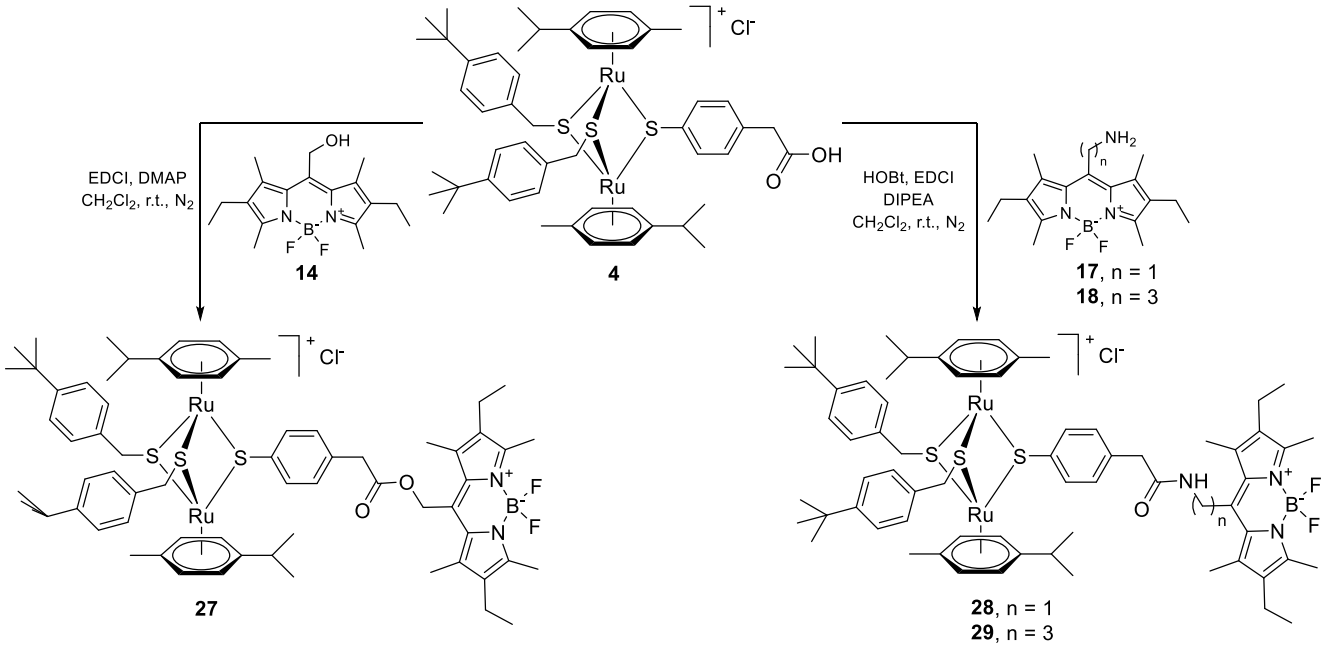

Scheme 5. Synthesis of the ester (left) and amide (right) conjugates BODIPY-dinuclear trithiolato ruthenium(II)-arene complexes **27**, **28** and **29** containing short alkyl spacers.

The ester conjugate **27** was obtained using EDCI as coupling agent and DMAP as base and was isolated in 35% yield. Amide dyads **28** and **29** were obtained in the presence of EDCI and HOBt as coupling agents and DIPEA as base and both were isolated in 52% yield.

To further vary the photophysical properties, the use of structurally different BODIPY dyes was also considered. BODIPY derivatives presenting an aromatic unit in the *meso*-position were largely studied and represent an interesting option.[19c]

BODIPY derivative **30** was synthesized by reacting 3-ethyl-2,4-dimethylpyrrole with 4-(chloromethyl)benzoyl chloride as acylium equivalent (Scheme 6). Addition of DIPEA to the intermediate acylpyrrole formed *in situ*, followed by application of $BF_3{\cdot}OEt_2$ afforded the BODIPY dye **30** isolated in 85% yield.

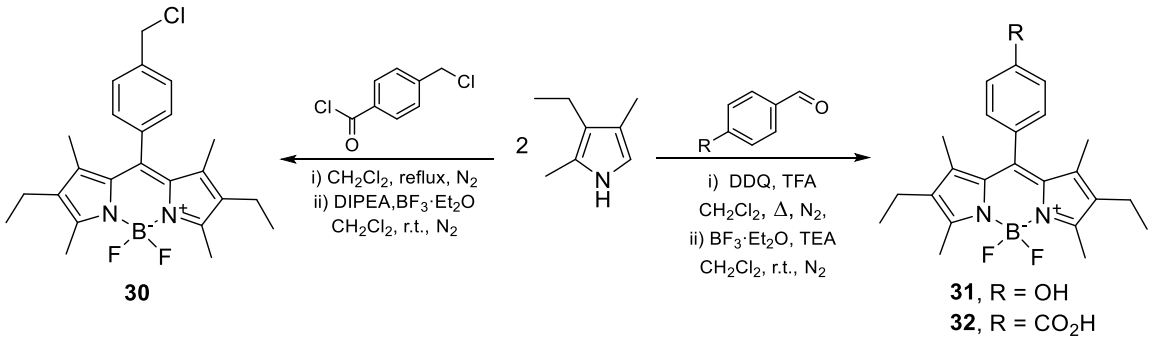

Scheme 6. Synthesis of the *meso*-arene BODIPY dyes **30**, **31** and **32** functionalized with chloromethylene, hydroxy and carboxy groups, respectively.

The condensation of pyrrole derivatives with aromatic aldehydes, followed by oxidation and complexation is a largely used method for the obtainment of *meso*-aryl BODIPY fluorophores,[52] which

led to abundant use of the *meso*-aryl group as a synthetic handle for the introduction of various functionalities.[53] The TFA (trifluoroacetic acid) catalyzed condensation of 4-hydroxybenzaldehyde and 4-carboxybenzaldehyde with 3-ethyl-2,4-dimethylpyrrole (Scheme 6) afforded the corresponding dipyrromethane intermediates (not isolated) which were further oxidated with DDQ (2,3-dichloro-5,6-dicyano-*p*-benzoquinone) to yield dipyrrin structures. The dipyrrins were subjected to TEA (triethylamine) and $BF_3{\cdot}OEt_2$ to afford the boron difluoride complexes **31** and **32** in low yield of 28 and 25%, respectively (Scheme 6).

Nucleophilic substitution of the chlorine atom in intermediate **30** with the diruthenium amino derivative **3** in the presence of KI as activator, in basic conditions (DIPEA) (Scheme 7 (top)), allowed the obtainment of the BODIPY amino conjugate **33** isolated in 50% yield. Hydroxy functionalized BODIPY derivative **31** was reacted with the diruthenium carboxy compound **4** using EDCI as coupling agent and DMAP as basic catalyst, to afford the ester conjugate **34** isolated in 30% yield (Scheme 7 (bottom)).

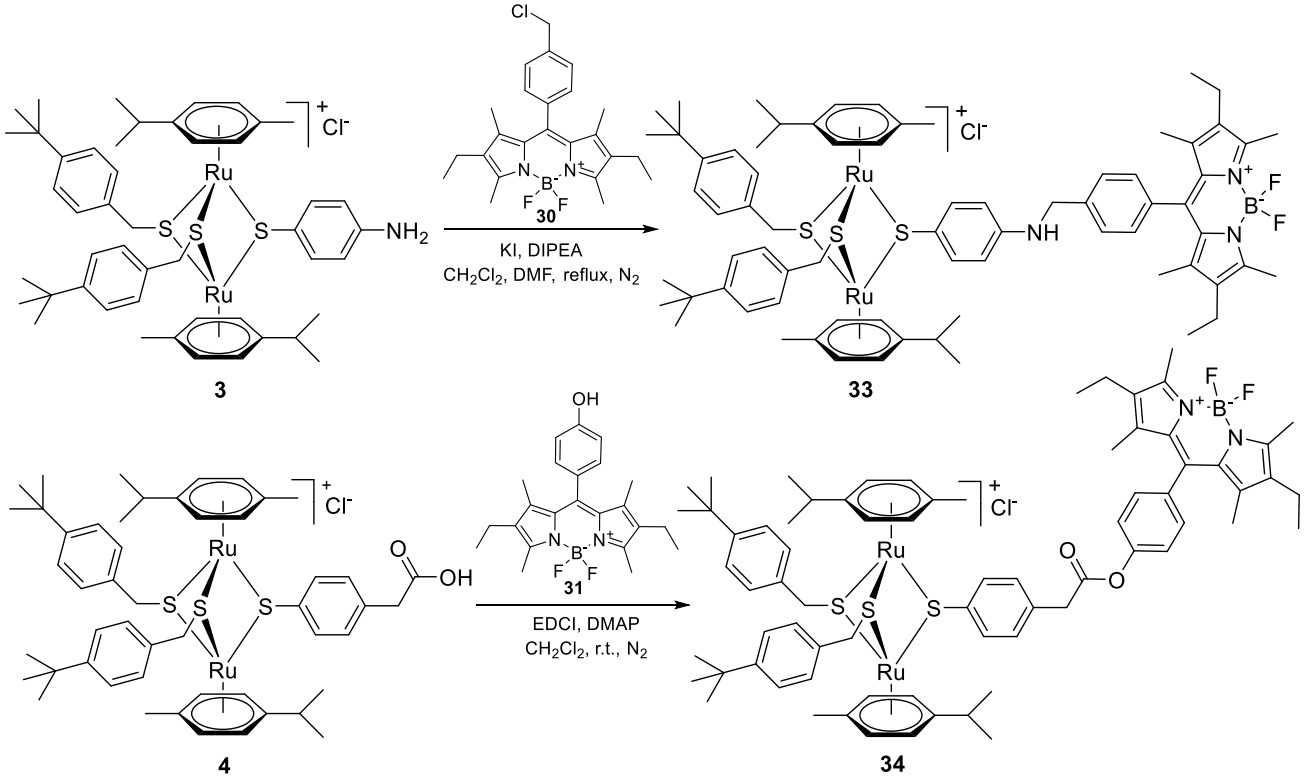

Scheme 7. Synthesis of the amine (top) and ester (bottom) conjugates *meso*-aryl BODIPY-dinuclear trithiolato ruthenium(II)-arene complexes **33** and **34**.

The carboxy *meso*-aryl BODIPY dye **32** was reacted with the diruthenium hydroxy and amine intermediates **2** and **3** leading to the obtainment of the ester and amide conjugates, **35** and, respectively, **36** (Scheme 8). In the first case, the reaction was run in the presence of EDCI as coupling agent and DMAP as basic catalyst and the ester dyad **35** was isolated in 25% yield. The synthesis of the amide analogue **36** was realized in the presence of EDCI and HOBt as coupling agents and of DIPEA as basic catalyst, the conjugate being isolated in 56% yield.

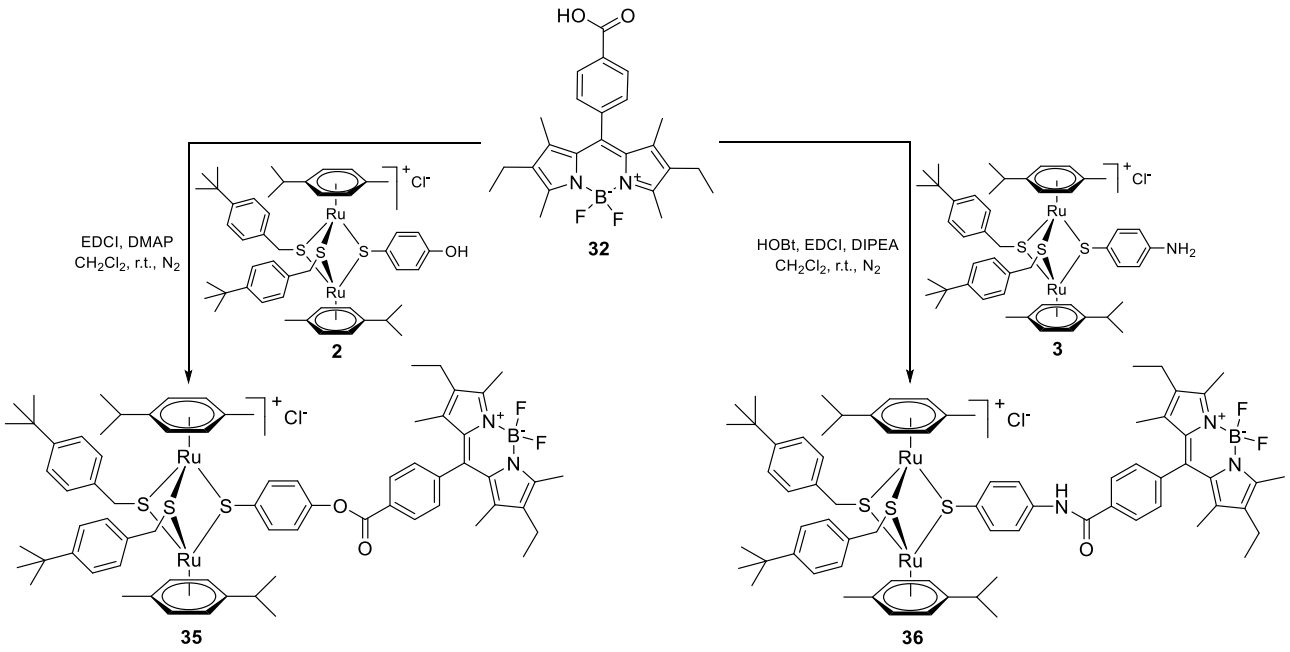

Scheme 8. Synthesis of the ester (left) and amide (right) dyads *meso*-aryl BODIPY-dinuclear trithiolato ruthenium(II)-arene complexes **35** and **36** .

All compounds were fully characterized by ^{1}H, ^{13}C and, where suitable, ^{19}F and ^{11}B nuclear magnetic resonance (NMR) spectroscopy, high resolution electrospray ionization mass spectrometry (HR ESI-MS) and elemental analysis (see the Experimental Section Chemistry in *Supporting Information* for full details). Mass spectrometry corroborated the spectroscopic data with the trithiolato diruthenium conjugates **19**-**29** and **33**-**36** exhibiting molecular ion peaks corresponding to $[M\text{-}Cl]^{+}$ ions.

For the assessment of the biological activity, the compounds were prepared as stock solutions in dimethylsulfoxide (DMSO), a solvent in which the derivatives present good solubility. Similarly, to previous reports[41, 45], ^{1}H-NMR spectra of conjugates **2**-**4**, **19**-**29** and **34** solubilized in DMSO-d_6, recorded at 25°C, 5 min and more than 1 month after sample preparation showed almost no changes (see Figures S6 and S8 in the *Supporting Information*), demonstrating the compounds high stability in this highly complexing solvent.

2.2. X-ray Crystallography

The crystal structures of BODIPY derivatives **16** and **30** were established in the solid state by single-crystal X-ray diffraction substantiating the expected structure (ORTEP representation are shown in Figure 2, see *Supporting information* for full experimental details and more related information). Data collection and refinement parameters are given in Table S2, whereas selected structural data are presented in Table 1.

Slow evaporation of solutions of **16** and **30** in $CHCl_3$ afforded pink-violet single crystals suitable for X-ray diffraction. The crystallographic data revealed that **16** crystallizes in the triclinic system, space group P-1, while **30** crystallizes in the monoclinic system, space group $P2_1/n$. In both structures, the central

six-membered ring of the BODIPY moiety is almost coplanar with the adjacent pyrrole rings, with a π-electron delocalization in the BODIPY core, as often observed for this class of compounds.[54] The two B–N distances are similar, while for N1–C1 and N2–C9 the measured bond lengths reveal a pronounced double bond character.

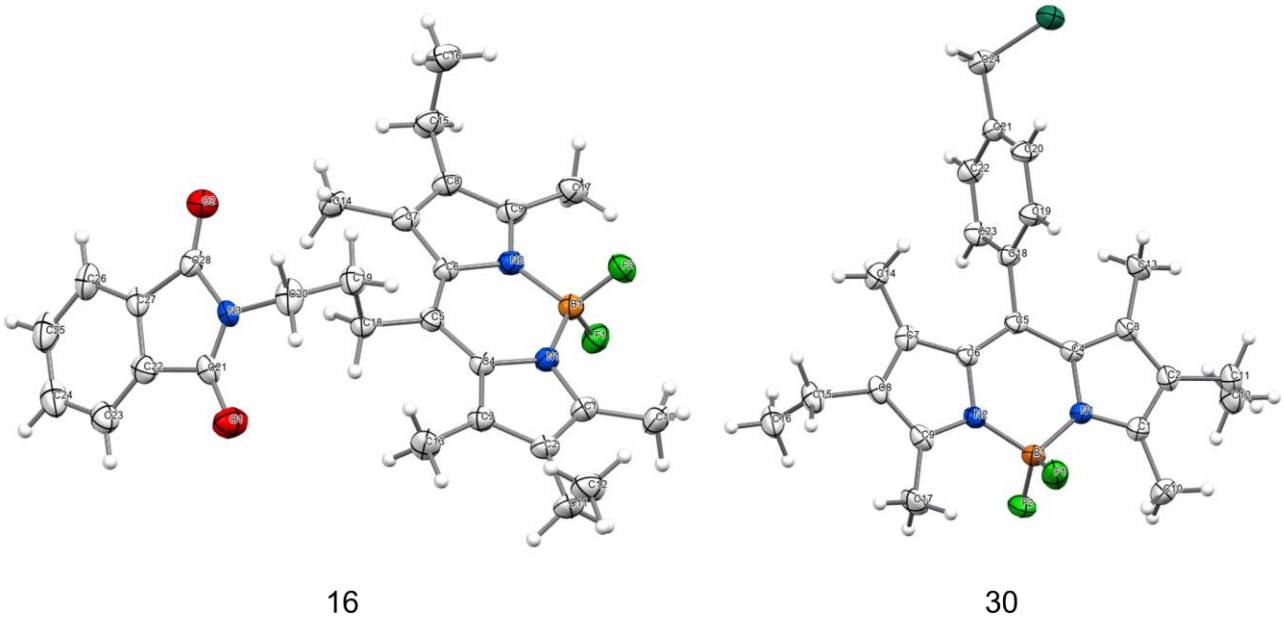

16 30

Figure 2. ORTEP representation of BODIPY derivatives **16** and **30** (thermals ellipsoids are shown with 50% probability).

Table 1. Selected structural parameters for the crystal structures of **16** and **30**.

Compound	B–N (Å)	B–F (Å)	N-C(CH_3) (Å)	N–B–N (°)	F–B–F (°)
16	N_1-B_1 1.5396(18) N_2-B_1 1.5399(18)	F_1-B_1 1.3947(17) F_2-B_1 1.3918(17)	N_1-C_1 1.3534(16) N_2-C_9 1.3456(16)	N_1-B_1-N_2 107.11(11)	F_2-B_1-F_1 108.47(11)
30	N_1-B_1 1.5472(19) N_2-B_1 1.543(2)	F_1-B_1 1.391(2) F_2-B_1 1.385(2)	N_1-C_1 1.3471(19) N_2-C_9 1.3505(18)	N_2-B_1-N1 106.87(11)	F_2-B_1-F_1 109.64(13)

2.3. Photophysical Properties

The photophysical properties of the BODIPY derivatives **5-18** and **30-32**, and of the conjugates BODIPY-trithiolato ruthenium(II)-arene complexes **19-29** and **33-36** are summarized in Table 2. The absorption and emission spectra of compounds **7**, **11**, **21**, **25**, **32**, **35** and **36** (10 μM solution in $CHCl_3$) are comparatively shown in Figures 3-5.

Table 2. Photophysical properties of compounds **5-36** (10 μM solution in $CHCl_3$).

Compound	λ_{max}^{Abs} (nm)	ε ($M^{-1}cm^{-1}$)	λ_{max}^{Em} (nm)	$\Delta\lambda$ (nm)	Φ_F (%)

Rhodamine 6G[a]	532.5	60832.8	557	24.5	75*
BODIPY derivatives with aliphatic handles					
5	527	62440.3	543	16	79
6	524	57593.2	538	14	82
7	523	71699.1	538	15	87
8	522.5	53674.9	537	14.5	84
9	526.5	35884.7	540	13.5	77
10	523.5	24534.4	536	12.5	92
11	523	55178.2	536	13	83
12	522.5	51363.4	537	14.5	86
13	549	36932.2	569	20	72
14	544.5	55663.2	565	20.5	64
15	546, 309.5	8045.19	554	8	14
16	525	46390.0	539	14	64
17	534	56442.9	551	17	78
18	527.5	43566.5	542	14.5	63
Diruthenium-BODIPY conjugates with aliphatic spacers					
19	529, 245	56519.5, 63901.6	543	14	11
20	524, 244.5	63619.5, 63006.0	539	15	17
21	523, 244.5	62739.9, 69086.4	538	15	14
22	522.5, 247	68351.7, 70393.6	538	15.5	18
23	524.5, 245.5	59063.5, 69777.7	540	15.5	12
24	521.5, 245	64531.5, 73078.6	536	14.5	12
25	521.5, 245	58855.7, 67572.0	536	14.5	14
26	521.5, 247.5	66142.7, 74163.7	536	14.5	18
27	536, 247.5	1598.3, 4660.3	552	16	10
28	539, 244.5	50505.5, 67274.0	556	17	5
29	521.5, 247.5	64983.9, 68330.6	537	15.5	6
BODIPY compounds with aromatic handles					
30	527.5	56484.9	544	16.5	63
31	525.5	59696.8	541	15.5	74
32	528.5	48019.8	547	18.5	40
Diruthenium-BODIPY conjugates with aromatic spacers					
33	526.5, 247.5	65652.2, 74004.7	545	18.5	6
34	527.5, 247.5	64733.1, 67122.7	545	17.5	15
35	529.5, 247.5	38450.4, 62860.5	548	18.5	17
36	527, 247.5	60159.8, 71312.0	544	17	19

[a]Values taken from ref.[55]

The BODIPY intermediates **5-8**, in which the ester group is separated from the dye moiety by aliphatic chains of different lengths, exhibit typical[19c] absorption and emission bands between 522-527 nm and 537-543 nm respectively, with high quantum yields (Φ_F = 77-87%). Slight hypsochromic shifts in both absorption and emission spectra can be observed after deprotection to acids **9-12**, with minor changes in quantum yields. Interestingly, the length of the spacer chain affects both the absorption and emission wavelength, with shorter chains leading to more important bathochromic shifts. For example, compounds **13-18** absorb at 525-549 nm, emit at 539-569 nm, and exhibit quantum yields lover (Φ_F = 63-78%) compared to derivatives with longer chains. Compound **15** shows a low quantum yield of 14%, probably due to the presence of the phthalimide group in close vicinity to the BODIPY unit. *Meso*-aryl compounds **30-32** absorb at 525-528 nm and emit at 541-547 nm. As expected,[19c] changing the nature of the *meso* substituent from aliphatic to aromatic neither affects the absorption nor the emission of BODIPYs, but the quantum yields are significantly lower (Φ_F = 40-74%).

As shown in Figures 3-5 and in accordance with previous reports (see selected photophysical parameters for various compounds in Figure 1), upon excitation at 450 nm, the conjugates **19-29** and **33-36** emitted at 500-570 nm (green area) due to the presence of the BODIPY chromophores. Absorption spectra of all dyads (**19-29** and **33-36**) are similar (Figures 3-5) and correspond well to an overlapping of the absorption spectra of the two units (diruthenium intermediates and BODIPY dyes), with strong peaks at 200-300 nm and 450-570 nm regions. With the exception of compounds **11**, **12** and **22**, the BODIPY derivatives and conjugates present rather comparable Stokes' shifts values between 13-16 nm (Table 2) similar to reported compounds.[53]

The introduction of the diruthenium moiety does not influence the absorption of the dye moiety, but however it induces an important fluorescence quenching irrespective of the nature of the polar group anchored on the BODIPY (e.g., CO_2H in **9-12**, OH in **14**, or NH_2 in **17-18**) or of the type of bond connecting the dyads' units (ester *vs* amide, e.g., **19-22**, **27** *vs* **23-26**, **28**, **29**). A less important quenching effect was observed in the case of conjugates **34-36** with more rigid *meso*-aryl BODIPY dyes. No direct correlation between the quenching intensity and length of the spacer was observed, even if shorter chains favor this outcome (e.g., **19**, **23-24**, **27-29**). A similar quenching effect was observed for formerly reported BODIPY-labelled metal complexes.[11c, 24b, 25a, 32, 35] This effect was explained by the fact that this type of compounds are prone to PET,[37] and that they can promote phosphorescence of the BODIPY unit.[38] In contrast, the fluorescence of a previously reported series of conjugates coumarin - trithiolato-bridged diruthenium complexes was almost completely quenched and the compounds could not be exploited for intracellular visualization.[41]

Despite a general substantial fluorescence quenching, a sufficient intense emission was measured for the dyads in solution, which enabled the study of compound **20** as potential tracking agents using fluorescence microscopy.

10.1002/cbic.202200536

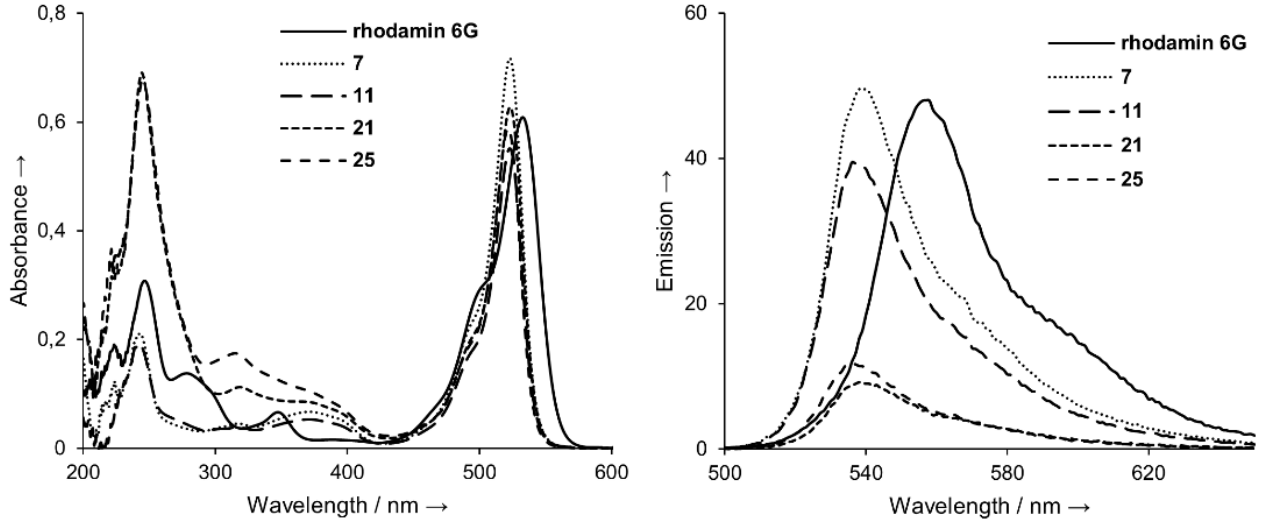

Figure 3. UV-Vis absorption (left) and emission spectra (right) of rhodamine 6G, BODIPY compounds **7**, **11**, and the corresponding ester **21** and amide **25** conjugates BODIPY - trithiolato diruthenium complex, at 10 μM in $CHCl_3$.

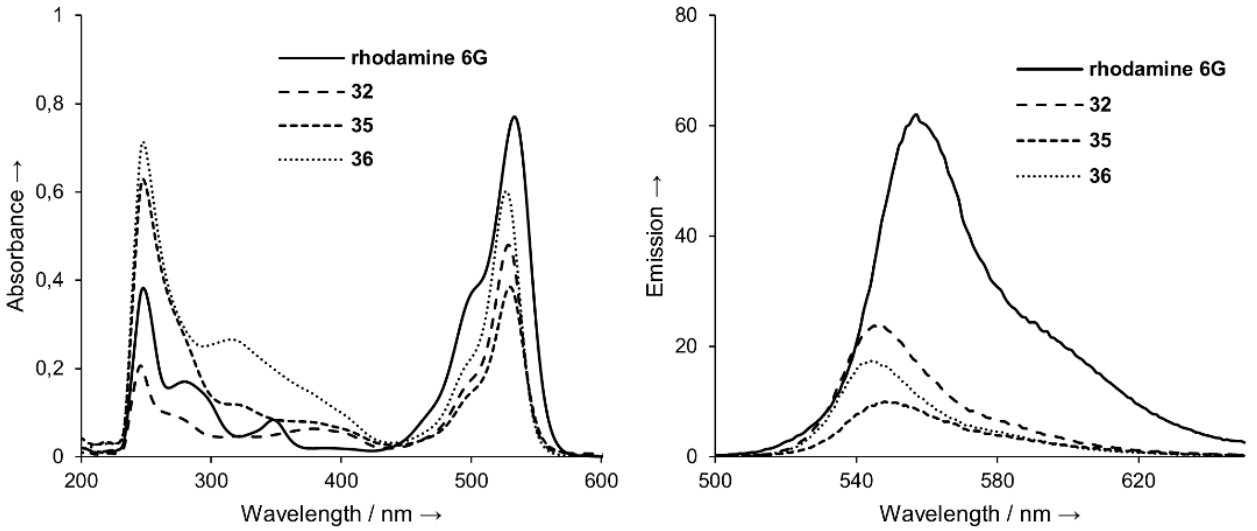

Figure 4. UV-Vis absorption (left) and emission spectra (right) of rhodamine 6G, BODIPY compound **32** and the corresponding ester **35** and amide **36** conjugates BODIPY - trithiolato diruthenium complex, at 10 μM in $CHCl_3$.

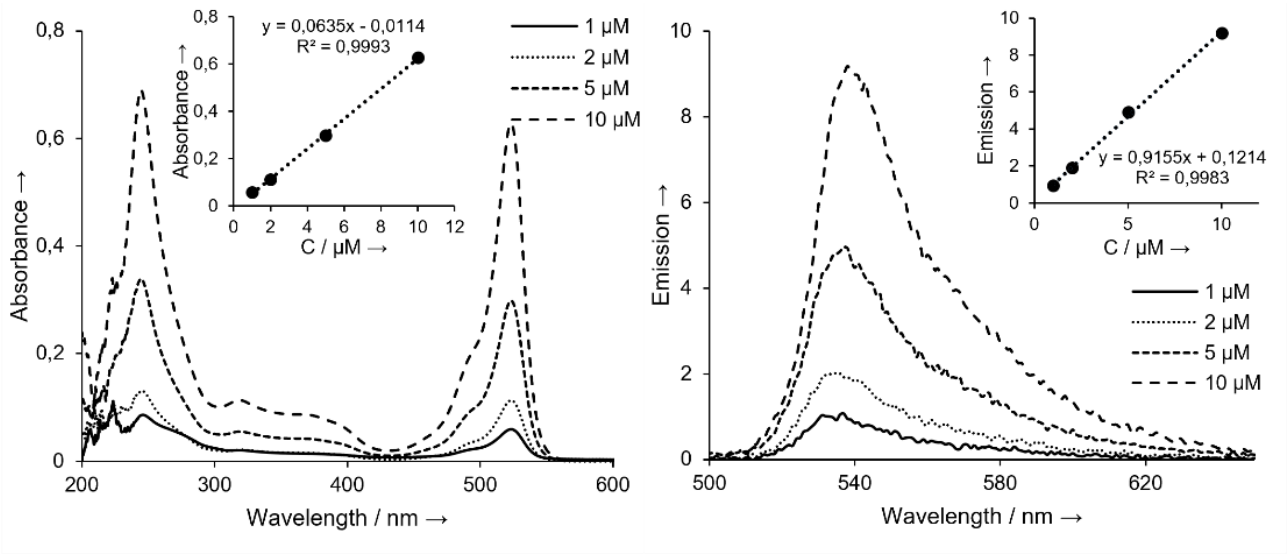

Figure 5. UV-Vis absorption (left) and emission spectra (right) of ester **21** conjugate BODIPY - trithiolato diruthenium complex at various concentrations in $CHCl_3$.

2.4. In vitro activity against T. gondii tachyzoites

The antiparasitic activity of all compounds regarding their ability to inhibit the *in vitro* proliferation of tachyzoites was evaluated on *T. gondii* β-gal (a transgenic strain constitutively expressing β-galactosidase) grown in HFF (human foreskin fibroblast) host cell monolayers. The cellular toxicity of these compounds was separately assessed on non-infected HFFs[6] and quantified by alamarBlue assay. The compounds (conjugates, BODIPY dyes and respective intermediates) were subjected to a sequential biological screening strategy already applied in previous studies.[45a] For the primary screening, cultures were exposed to 0.1 and 1 µM of each compound for 72 h. As controls (100% viability and 100% proliferation), non-infected HFF and *T. gondii* infected HFF cultures were treated with 0.1% DMSO. In the second screening, the selected compounds (molecules that when applied at 1 µM inhibited *T. gondii* β-gal proliferation by at least 90% and did not impair HFF viability by more than 50%) were submitted to dose response studies to determine the IC_{50} values, while cytotoxicity in HFF was assessed at 2.5 µM. The non-modified trithiolato-bridged dinuclear ruthenium(II)-arene complexes **2-4** were formerly evaluated against *T. gondii* β-gal under identical conditions,[41, 45] and the corresponding values were provided for comparison in Table 3 and Figure 6. The library of tested compounds included the BODIPY dyes and the corresponding intermediates **5**-**18** and **30**-**32** (results summarized in Table S1 and Figure S1 in *Supporting information*) and the diruthenium-BODIPY conjugates with aliphatic and aromatic spacers **19**-**29** and, respectively, **33**-**36** (Table 3 and Figure 6).

Table 3. Primary efficacy/cytotoxicity screening of the diruthenium compounds in non-infected HFF cultures and *T. gondii* β-gal tachyzoites cultured in HFF monolayers. The compounds selected for the determination of IC_{50} values against *T. gondii* β-gal are tagged with *.

Compound	HFF viability (%)	*T. gondii* β-gal growth (%)

	0.1 μM	1 μM	0.1 μM	1 μM
Diruthenium intermediates				
2[a],*	76 ± 6	46 ± 6	66 ± 14	2 ± 0
3[a],*	74 ± 2	48 ± 1	57 ± 1	2 ± 0
4[a],*	91 ± 4	73 ± 1	114 ± 2	110 ± 2
Diruthenium-BODIPY conjugates with aliphatic spacers				
19*	99 ± 5	87 ± 7	13 ± 2	0 ± 0
20*	102 ± 2	83 ± 4	74 ± 4	0 ± 0
21*	102 ± 2	75 ± 11	22 ± 0	0 ± 0
22*	97 ± 11	94 ± 7	40 ± 5	0 ± 1
23	106 ± 0	96 ± 1	33 ± 4	11 ± 2
24	106 ± 3	99 ± 1	125 ± 9	70 ± 6
25	98 ± 16	100 ± 1	122 ± 9	101 ± 8
26	84 ± 1	71 ± 4	94 ± 5	83 ± 7
27*	107 ± 5	97 ± 3	126 ± 16	1 ± 1
28*	105 ± 1	102 ± 0	113 ± 7	1 ± 1
29	107 ± 3	101 ± 1	85 ± 9	76 ± 13
Diruthenium-BODIPY conjugates with aromatic spacers				
33*	100 ± 3	93 ± 1	123 ± 7	0 ± 0
34	126 ± 4	129 ± 3	140 ± 1	62 ± 1
35	110 ± 4	108 ± 2	85 ± 4	28 ± 2
36	102 ± 1	93 ± 2	105 ± 2	76 ± 3

[a]Data for compounds **2-4** were previously reported.[45a]

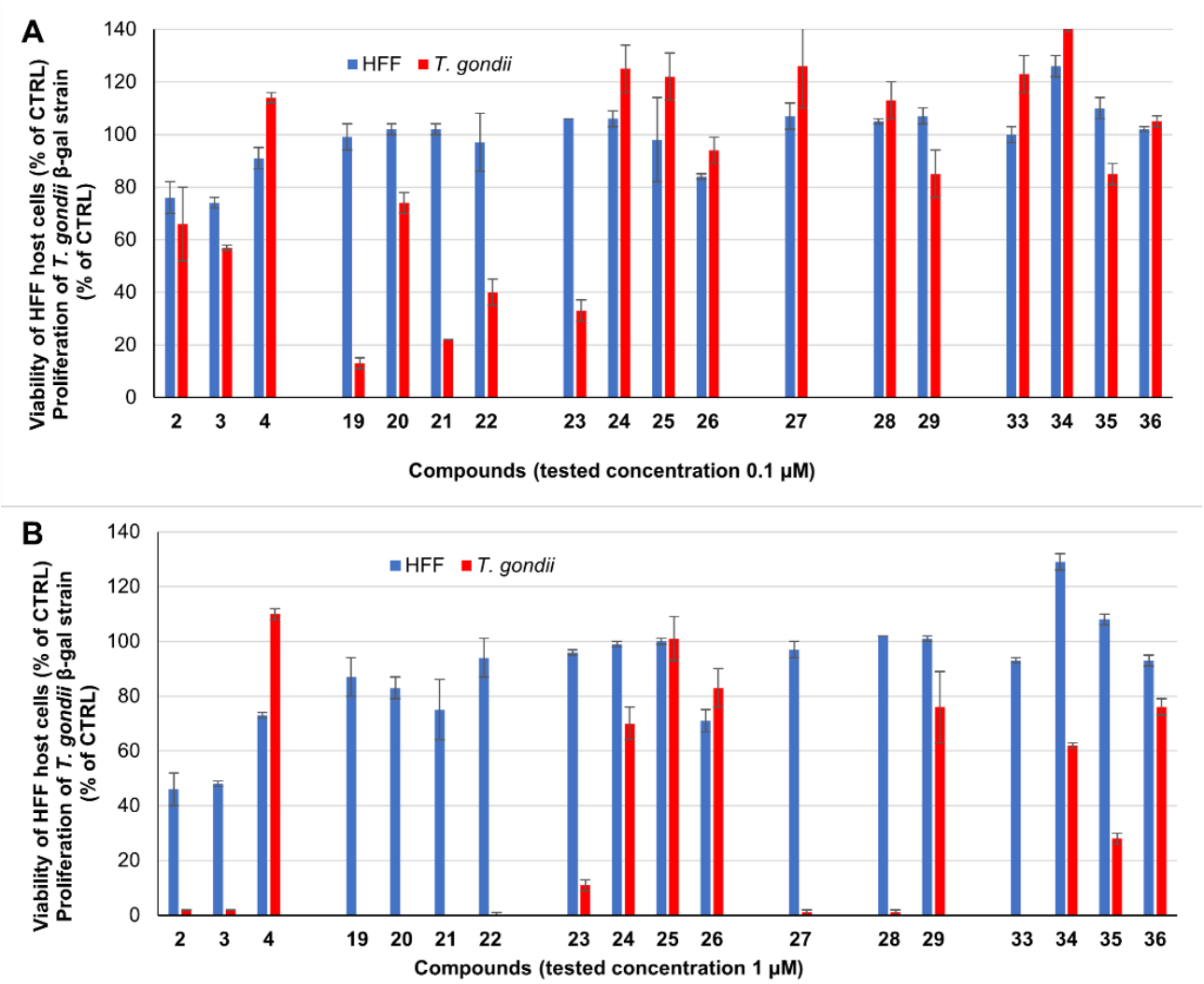

Figure 6. Clustered column chart showing the *in vitro* activities at 0.1 (A) and 1 (B) µM of the trithiolato diruthenium compounds on HFF viability and *T. gondii* β-gal proliferation. As controls (100% viability and 100% proliferation), non-infected HFF and *T. gondii* infected HFF cultures were treated with 0.1% DMSO. For each assay, standard deviations calculated from triplicates are displayed on the graph. Data for compounds **2-4** were previously reported.[45a]

The biological activity of the hydroxy, amino and carboxy diruthenium compounds **2-4** was investigated in a former study.[45a] While **4** had very limited effect on HFF and parasites at both concentrations, **2** and **3** at 1 µM almost completely abolished parasite proliferation but also exhibited considerable cytotoxicity.

Both esters **19-22** and amide analogues **23-26** exerted limited cytotoxicity when applied at 1 µM. However, ester derivatives **19-22** were significantly more efficient in inhibiting *T. gondii* β-gal proliferation compared to the respective amides **23-26** especially when applied at 1 µM. Conjugates **19-22** also appear to be more active and less toxic compared to corresponding hydroxy intermediate **2**. Only amide **23** exhibited some activity against *T. gondii*, while derivatives **24-26** with longer spacers between the BODIPY and the diruthenium unit did not affect the parasite proliferation. Amide **23** presented an

improved activity/cytotoxicity profile as well compared to the respective diruthenium amino intermediate **3**.

For conjugates **27**, **28** and **29**, both the nature of the bond between the two units and the length of the spacer strongly influenced the biological activity. Neither ester **27** nor its structurally related amide **28** affected the host cell viability even when applied at 1 μM, while both compounds completely inhibited parasite proliferation at the same concentration. Like the corresponding diruthenium carboxy intermediate **4**, amide **29** did not exhibit cytotoxicity or antiparasitic effects at both tested concentrations. Conjugates **33**-**36**, in which the fluorophore presents a *meso*-aryl handle, did not affect HFF viability at the tested concentrations and, except for amino-linked compound **33**, they demonstrated only poor anti-*Toxoplasma* efficacy.

When applied at 1 μM, all BODIPY intermediates and dyes exhibited negligible effect on *T. gondii* β-gal proliferation and, apart from derivative **6**, they did not affect the host cell proliferation by more than 50% at the same concentration (Table S1 and Figure S1).

Seven new diruthenium-BODIPY conjugates fulfilled the selection criteria (compounds that when applied at 1 μM inhibited *T. gondii* β-gal proliferation by at least 90% and did not impair HFF viability by more than 50%) and were submitted to a second screening IC_{50} determination on *T. gondii* and toxicity assessment to host cells at 2.5 μM (Table 4).

Table 4. *T. gondii* β-gal half-maximal inhibitory concentration (IC_{50}) values (μM) and viability of HFF cultures exposed to 2.5 μM for seven selected diruthenium-BODIPY conjugates, standard drug pyrimethamine and diruthenium intermediates **2** and **3**.

Compound	IC_{50} (μM)	[LS; LI][b]	SE[c]	HFF viability at 2.5 μM (%)[d]	SD[e]
Pyrimethamine[a]	0.326	[0.396; 0.288]	0.052	99	6
Diruthenium intermediates					
2[a]	0.117	[0.139; 0.098]	0.051	56	6
3[a]	0.153	[0.185; 0.127]	0.049	51	5
Diruthenium-BODIPY conjugates with aliphatic spacers					
19	0.442	[0.524; 0.373]	0.169	79	0
20	0.483	[0.613; 0.381]	0.238	91	0
21	0.255	[0.272; 0.240]	0.060	93	0
22	0.419	[0.518; 0.339]	0.211	95	0
27	0.524	[0.555; 0.495]	0.057	91	0
28	0.385	[0.576; 0.257]	0.156	86	0
Diruthenium-BODIPY conjugates with aromatic spacers					
33	0.512	[0.678; 0.387]	0.110	96	0

[a]Data for pyrimethamine, **2** and **3** were previously reported;[45a] **2** and **3** do not correspond to the first screening selection criteria, but the IC_{50} values and viability of HFF were determined for comparison purpose. [b]Values at 95% confidence interval (CI); LS is the upper limit of CI and LI is the lower limit of CI. [c]The standard error of the regression (SE), represents the average distance that the observed values fall from the regression line. [d]Control HFF cells treated only with 0.25% DMSO exhibited 100% viability. [e]Standard deviation of the mean (six replicate experiments).

The selected conjugates exhibit IC_{50} values against *T. gondii* β-gal ranging from 0.255-0.524 μM, which are lower compared to formerly reported diruthenium complexes[6, 45a] or hybrid molecules in which the this organometallic moiety was functionalized with coumarin fluorophores[41] or with antimicrobial drugs.[42] This substantiates the critical role of the organic fragment appended to the diruthenium scaffold for the overall biological activity of the conjugates.

Dyads **19**, **21**, **22** and **28** had a similar impact on *in vitro* proliferation of *T. gondii* to that exerted by pyrimethamine (IC_{50} = 0.326 μM), a standard treatment for toxoplasmosis. For **19**, **21**, **22** and **28** the cytotoxicity against HFF was in a close range (79-95%) and comparable to that of pyrimethamine (99%). Conjugation of BODIPY dyes to the diruthenium moiety resulted in a significantly reduced cellular toxicity compared to corresponding hydroxy and amino functionalized diruthenium intermediates **2** and **3**.

Overall, the screening results indicate that the potential of the BODIPY-diruthenium hybrids as antiparasitic therapeutic agents is moderate. Among the newly reported compounds, conjugate **21** exhibits the lowest IC_{50} value (0.255 μM). Yet, **21** is less active than the hydroxy diruthenium intermediate **2** but exhibits also lower toxicity to host cells.

Nonetheless, this type of dyads could be of potential interest as fluorescent probes for tracking their uptake and localization in cells and parasites.

2.5. Transmission electron microscopy

The ultrastructural changes induced by BODIPY ester conjugates **21** and **27** (presenting the lowest and the higher IC_{50} values against *T. gondii* β-gal from the current compound library) were studied by TEM. HFF monolayers were infected with *T. gondii* β-gal tachyzoites, and compounds were added after the infection was established. The cultures were either maintained as controls without addition of compounds (Figure 7), or at 24 h post-infection, treatments with **21** or **27** (administrated at 0.5 μM) were initiated (Figure 8). In all cases, cultures were fixed and processed for TEM at 48 h post-infection. In control cultures (Figure 7), *T. gondii* tachyzoites were found to be located within the cytoplasm of their host cells, within a parasitophorous vacuole that was delineated by a parasitophorous vacuole membrane. At 24 h post-infection, vacuoles contained mostly 2 tachyzoites (Figure 7A), while at 48 h, proliferation had resulted in larger vacuoles with an increased number of tachyzoites (Figure 7B). Proliferation of

T. gondii takes place by endodyogeny, thus two daughter zoites emerge from one tachyzoite, as indicated in Figure 7C.

In non-treated parasites, the nucleus (nuc), and secretory organelles such as micronemes (mic) and dense granules (dg) are clearly visible. Host cell mitochondria (hmito) are often found in the close vicinity of the parasitophorous vacuole membrane. Tachyzoites contain one mitochondrion (mito) that forms an intracytoplasmic tubular network, of which are visible only the parts exposed on the surface of the section plane (Figure 7C). The matrix of the mitochondrion is electron-dense and contains numerous cristae.

After exposure of *T. gondii*-infected HFF to 0.5 μM of **21** for 24 h (Figure 8 A-D), profound changes occurred most notably in the matrix of the tachyzoite mitochondrion, as indicated by the red frames. In many instances, the mitochondrial matrix was dissolved, with only remnants of cristae found within otherwise empty vacuoles. However, these changes were not evident in all domains of the mitochondrion, as can be seen in Figure 8B (framed in yellow). Mitochondrial alterations were less pronounced compared to similar modifications induced by coumarin-trithiolato diruthenium conjugates[41] or by other complexes with no organic molecule appended on one of the bridging thiols.[6] In addition, mitochondrial changes were not as readily identified upon treatment with compound **27**, for which the impact on the mitochondrial matrix was evident only in about 20% of tachyzoites (Figure 8 E, H). Overall, the shape and size of the parasites was not extensively altered by any of the two compounds. Additionally, the fact that parasites undergoing endodyogeny were readily identified, especially in compound **27** treated cultures (Figure 8 E, G), and larger vacuoles were seen in cultures treated with both compounds (Figure 8 A, E, F), show that these BODIPY-diruthenium conjugates did not have a notable impact on intracellular proliferation when applied after the infection has already been established.

10.1002/cbic.202200536

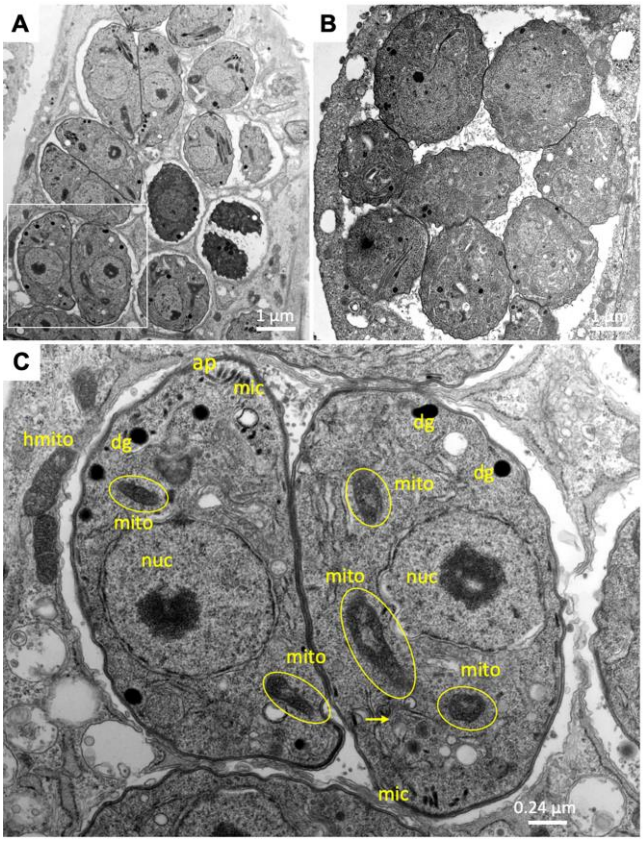

Figure 7. TEM of *T. gondii* β-gal tachyzoites fixed at 24 h post infection (A, C) and at 48 h post infection (B). A shows a low magnification view of several parasitophorous vacuoles within HFF host cells, a higher magnification view of the boxed area is shown in C. Tachyzoites proliferate by endodyogeny, and an emerging daughter zoites is indicated with the arrow. ap = apical part, mic = micronemes, dg = dense granules, mito = tachyzoite mitochondrion, hmito = host cell mitochondrion. Note the higher number of parasites within the parasitophorus vacuole fixed at 48 h. The yellow frames indicate the position of the visible parts of the mitochondrion.

10.1002/cbic.202200536

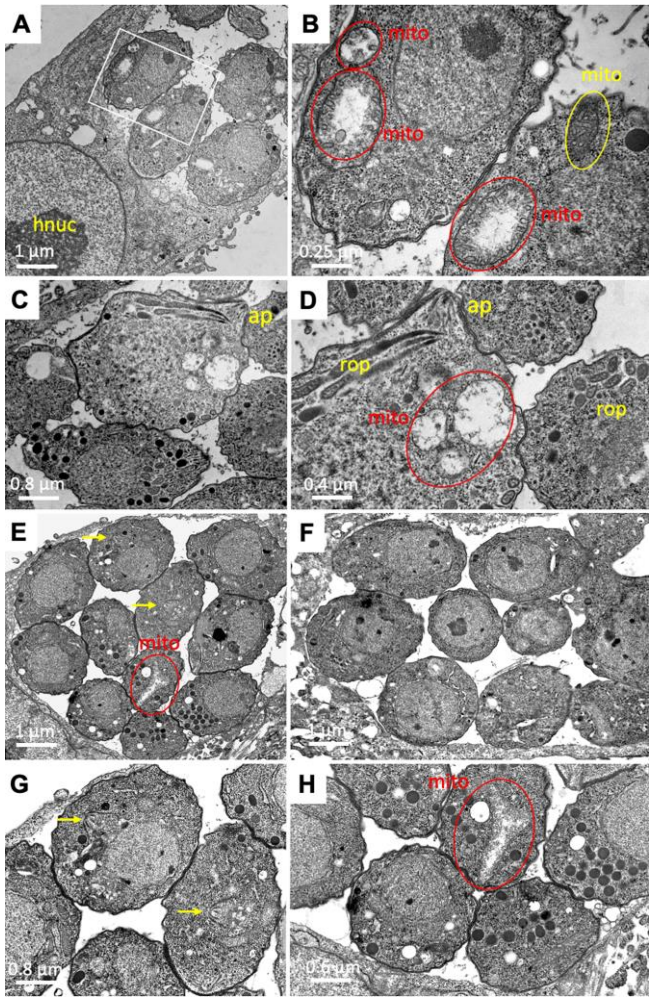

Figure 8. TEM of *T. gondii* β-gal tachyzoites treated with 0.5 µM of **21** (A-D) and 0.5 µM of **27** (E-H) fixed and processed 24 h after treatment initiation. A and C show lower magnification views of cultures treated with **21**, the boxed area in A is enlarged in B, and a parasite exhibiting profound changes in the mitochondrion (mito) is enlarged in D. Note that matrix remnants are more clearly detectable in B than in D. Larger parasitophorous vacuoles are found in cultures treated with **27** (E, F), and only few changes in the mitochondrion are evident (E, H). Arrows point towards parasites undergoing endodyogeny, ap = apical part, rop = rhoptries. Red frames indicate damaged parts of the mitochondrion, yellow frame shows a part of the mitochondrion with an intact matrix.

2.6. Fluorescence microscopy

To assess the potential use of the new conjugates BODIPY-diruthenium unit as cellular traceable probes and to identify possible key targets, fluorescence microscopy was performed on HFF treated with 20 µM of either carboxy BODIPY dye **10** or the corresponding BODIPY-diruthenium conjugate **20**. The microtubules of HFF were labelled with mouse monoclonal anti-alpha-tubulin antibody (Red) and DAPI (Blue) was used for staining the nuclei.

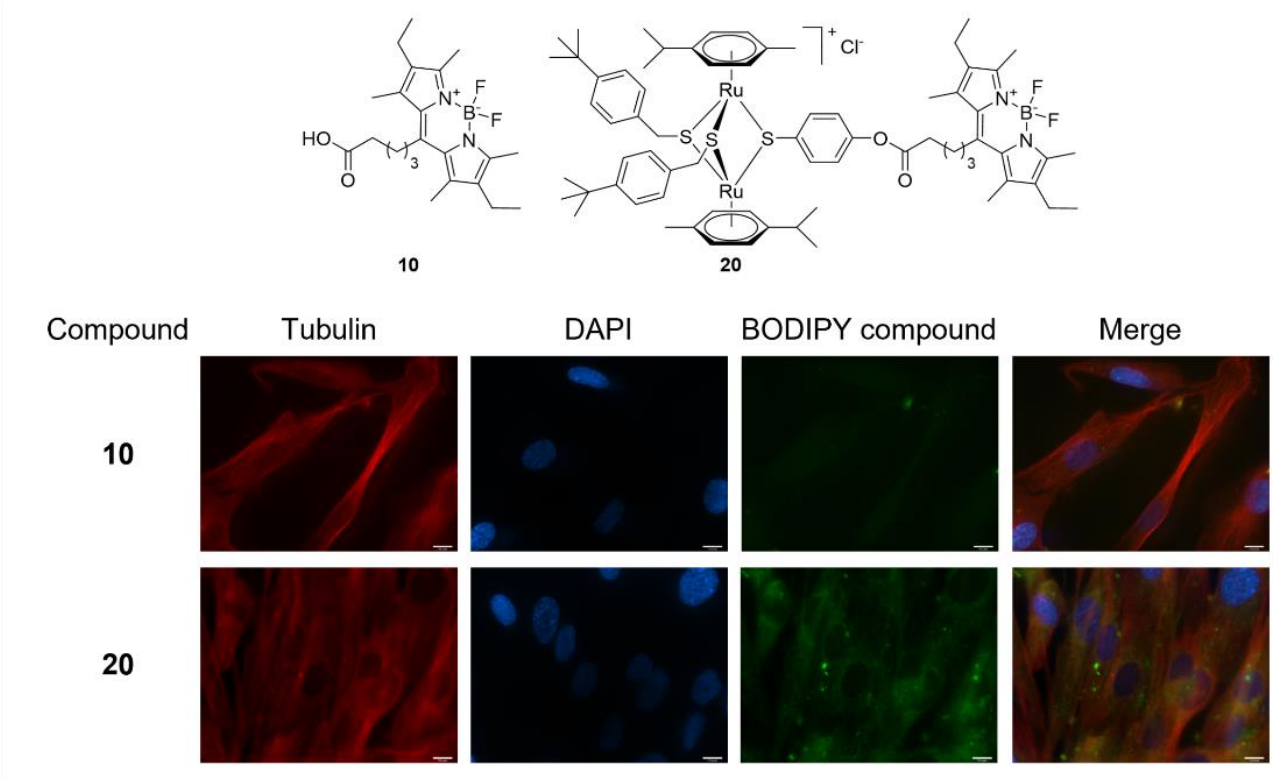

Figure 9. Fluorescence microscopy (green) of HFF treated with 20 µM of the BODIPY dye **10**, or the corresponding diruthenium conjugate **20** for 1 h at 37°C. Cells were stained with monoclonal anti-alpha-tubulin antibody (red) and DAPI (blue).

Interestingly, the fluorescence intensity of conjugate **20** inside the cells was greater compared to that of the corresponding BODIPY dye **10** (Figure 9), although the latter exhibits a significantly higher fluorescence quantum yield (Table 2). These results suggest that the BODIPY dye **10** was better taken up by HFF when it was conjugated to the diruthenium complex, which might indicate a higher internalization and/or a retention of the dyad **20**. A similar effect was reported for other hybrids metal complex-BODIPY dyes.[30, 35] As demonstrated in the merged image and in accordance with previous studies,[25a] within HFF **20** showed a pattern of cytoplasmic, but not nuclear, localization. This is despite the cationic nature of the diruthenium moiety which can interact with anionic molecules like DNA. The images suggest a localization of conjugate **20** on the HFF microtubules. Additional experiments are needed to corroborate these results but are beyond the scope of the current study.

3. Conclusions

A series of 15 new conjugates BODIPY-trithiolato-bridged dinuclear ruthenium(II)-arene complex were synthesized and fully characterized. The influence of the connecting bond (amide *vs* ester), as well as that of the type and length of the spacer between the dyads' units upon the photophysical and biological properties were evaluated.

The considered structural variations, as the connecting bond, the aliphatic spacer's length, the presence of an *meso*-aromatic ring in the BODIPY, had significant impact on both the conjugates' fluorescence

and measured antiparasitic properties, while they influenced in a lower extent the cytotoxicity (most dyads had negligible effect on HFF viability even at 1 μM). For example, when applied at 1 μM the ester conjugates with aliphatic spacers **19**-**22** exhibited noteworthy higher *T. gondii* antiproliferative activity compared to the corresponding amide analogues **23**-**26**.

Despite an important fluorescence quenching due to the conjugation of the BODIPY to the diruthenium unit, the spectral properties of the dyad **20** (relative Φ_F = 17%) allowed fluorescence microscopy visualization in HFF cells. Noteworthy, the intracellular fluorescence intensity was higher for conjugate **20** compared to that of the free BODIPY dye **10**, suggesting a better internalization and/or retention of the diruthenium conjugate.

The antiparasitic activity of the conjugates (in terms of IC_{50} values against *T. gondii*) remained in the same range as that of the standard drug pyrimethamine. Thus, while these compounds could be valuable fluorescent probes for tracking their cellular targets, their potential as antiparasitic therapeutic agents is moderate. However, the present biological evaluation results must be considered with caution, as it cannot be excluded that the cellular uptake, accumulation, and localization of the BODIPY dyads could diverge from those of non-modified diruthenium complexes or of other reported conjugates. Incidentally, TEM also points out the parasite mitochondrion as a potential target, but the observed effects were less pronounced compared to those of previously described trithiolato-bridged dinuclear ruthenium(II)-arene compounds and diruthenium conjugates. Additional experiments on cancer cells and bacteria using these BODIPY-diruthenium dyads as intracellular tracking agents are considered.

Experimental part

Chemistry

The chemistry experimental part, with full description of synthetic procedures and characterization data for all compounds, as well as the data corresponding to the crystal structures determination are presented in the *Supporting information*.

Photophysical measurements

Instruments and methods

UV-Visible spectra were recorded on a Thermo Scientific Evolution 201 UV-Vis spectrophotometer, and the fluorescence emission spectra were recorded on an Agilent Cary Eclipse fluorescence spectrophotometer. The UV-Vis absorption spectra of compounds **5**-**36** were recorded in the 200-1100 nm range at r.t. using 1, 2, 5 and 10 μM solutions in $CHCl_3$. Emission spectra were recorded in the 450-650 nm range after excitation at 450 nm at r.t. using the same solutions (1, 2, 5 and 10 μM solutions in $CHCl_3$).

Determination of quantum yields

Relative quantum yields in $CHCl_3$ at r.t. were calculated using equation (**1**) and rhodamine 6G (suitable for fluorescence, BioReagent, Sigma-Aldrich, Germany) (Φ_F = 0.75 in $CHCl_3$) as standard.[55]

$$\Phi_F(x) = \frac{A_s}{A_x} \times \frac{F_x}{F_s} \times \left(\frac{n_x}{n_s}\right)^2 \times \Phi_F(s) \quad (\mathbf{1})$$

where *A* is the absorbance at the excitation wavelength, *F* is the area under the emission curve, *n* is the refractive index of the solvent (at 20°C) used in measurements (n = 1.446 for $CHCl_3$), and the subscripts *s* and *x* represent standard and unknown, respectively.

Stokes shifts were calculated using equation (**2**) as the difference between the values of maxima of the intense bands in the fluorescence and absorption spectra:

$$\Delta\lambda = \lambda_{max}^{em} - \lambda_{max}^{abs} (\mathbf{2})$$

Biological activity evaluation

In vitro activity assessment against T. gondii tachyzoites and HFF

During the *in vitro* experimental testing, compounds were protected from the light. All tissue culture media were purchased from Gibco-BRL, and biochemical agents from Sigma-Aldrich. Human foreskin fibroblasts (HFF) were purchased from ATCC, maintained in DMEM (Dulbecco's Modified Eagle's Medium) supplemented with 10% fetal calf serum (FCS, Gibco-BRL, Waltham, MA, USA) and antibiotics as previously described[3e]. Transgenic *T. gondii* β-gal samples (expressing the β-galactosidase gene from *Escherichia coli*) were kindly provided by Prof. David Sibley (Washington University, St. Louis, MO, USA) and were *in vitro* maintained by serial passage in HFF as previously described[3e, 58].

All the compounds were prepared as 1 mM stock solutions from powder in dimethyl sulfoxide (DMSO, Sigma, St. Louis, MO, USA). For *in vitro* activity and cytotoxicity assays, HFF were seeded in 96 well plates at 5×10^3 /well and incubated at 37°C with 5% CO_2 until reaching confluency.

To measure proliferation of *T. gondii* β-gal tachyzoites in presence or absence of compounds, the β-galactosidase colorimetric assay was performed as previously described.[3e, 41-42, 45a] Briefly, experiments were conducted in 96 well plates, compounds were evaluated at 0.1 and 1 μM and added to HFFs prior to the infection with freshly isolated tachyzoites (1×10^3/well). Control untreated parasites received only media containing 0.01 or 0.1% DMSO. All cultures were incubated for 3 days at 37°C with 5% CO_2[45b]. At the end of the treatment, medium was removed, and cells were lysed with 0.05% Triton X-100 in phosphate-buffered saline (PBS) and 5 mM chlorophenol red-β-D-galactopyranoside (CPRG; Roche Diagnostics, Rotkreuz, Switzerland), the substrate for β-galactosidase was added. Absorbance of released chlorophenol red was measured at 570 nm using an EnSpire® multimode plate reader (PerkinElmer, Inc., Waltham, MA, USA). The 100% of proliferation was settled to the control untreated *T. gondii* β-gal-infected HFF.

IC_{50} determination on *T. gondii* β-gal was performed as previously described[41-42, 45a] based on the β-galactosidase colorimetric assay and by applying a range of concentrations from 0.007 to 1 μM. IC_{50} values were calculated after the logit-log-transformation of relative growth and subsequent regression analysis.

The cytotoxicity of the compounds on non-infected HFF was assessed by the Resazurin reduction assay (alamarBlue) as previously reported.[41-42, 45a, 59] Briefly, confluent HFF monolayer cultures in 96 well plates were exposed to 0.1, 1 and 2.5 μM of each compound. Non-treated HFF as well as DMSO controls (0.01%, 0.1% and 0.25%) were included. After 72 h of incubation at 37°C/5% CO_2, the medium was removed, and plates were washed three times with PBS. Then, 200 μL of resazurin (0.01 g/L) were added to each well. Fluorescent resorufin were measured at excitation wavelength 530 nm and emission wavelength 590 nM on an EnSpire® multimode plate reader (PerkinElmer, Inc.). Fluorescence was measured at two time points: 0 min (T0) and after 5 hours (T5h). After subtraction of T0 values from T5h, mean fluorescence and the standard deviation are calculated from three (primary screening) or six (secondary screening) replicates. The 100% viability was settled to control untreated HFF incubated in DMEM complemented medium containing 0.01%, 0.1% or 0.25% DMSO.

Transmission electron microscopy (TEM)

Transmission electron microscopy (TEM) was performed as previously described.[57] In brief, confluent HFFs grown in T25 flasks were infected with 10^6 *T. gondii* ME49 tachyzoites,(genotype II, kindly provided from Dr. Furio Spano, Istituto Superiore di Sanità, Roma, Italia) and 0.5 μM solutions of **21** or **27** were added at 24 h post-infection. After 24 and 48 h, medium from the flasks was discarded, cells were washed with a 0.1 M sodium cacodylate buffer (pH 7.3) and then fixed in 2% glutaraldehyde in cacodylate buffer for 10 min at room temperature r.t.. Fixed cultures were then gently scraped, transferred into Eppendorf tubes and fixed for another 2 h at r.t.. Specimens were then washed in cacodylate buffer, post-fixed in 2% osmium tetroxide in cacodylate buffer for 2 h at r.t.. Samples were then washed with water, pre-stained in saturated uranyl acetate solution and stepwise dehydration in ethanol. They were then embedded in Epon 812-resin, and processed for TEM as described.[6] Specimens were viewed on a CM12 transmission electron microscope operating at 80 kV.

Fluorescence microscopy

Glass cover slips of 12 mm in diameter were placed in 24 well culture plate and sterilized in UV Stratalinker 1800 (Stratagene) for 40 min. Cover slips were then coated with HFFs (2×10^4 cells/mL) and incubated for 3 days at 37°C with 5% CO_2. Afterwards, the culture medium was removed and replaced with fresh medium (1 mL/well) containing either (i) 0.5% DMSO, or (ii) 20 μM of BODIPY dye **10**, or (iii) 20 μM of ester conjugate **20**, the treatment duration being 1 h at 37°C/5% CO_2. After treatment,

wells were washed (3 washes with sterile PBS), fixed with 2% paraformaldehyde (PFA) in PBS for 20 min and permeabilized with 0.2% Triton X-100 in PBS applied for 5 min. Unspecific binding sites were blocked using 3% BSA in PBS for 2 h at r.t.. Glass coverslips were then incubated for 30 min with mouse monoclonal anti-alpha tubulin antibody (Sigma) diluted 1:200 in PBS containing 0.3% BSA, then with a goat anti-mouse antibody conjugated to TRITC (tetramethylrhodamine isothiocyanate) (Sigma, 1:200), and after three washes in PBS, coverslips were mounted in Vectashield plus DAPI and viewed on a Nikon Eclipse E800 digital confocal fluorescence microscope. Images were acquired and processed with Openlab 5.5.2 software.

Supplementary Materials: The *Supporting Information* is available online at www... Primary cytotoxicity/efficacy screening of BODIPY compounds **5**-**18** and **30**-**32** in non-infected HFF cultures and *T. gondii* β-gal tachyzoites cultured in HFF, crystal data and structure refinement for **16** and **30**, chemistry experimental part with the full description of experimental procedures, stability of compounds **2**-**4** and **15**-**21** in DMSO-d_6. Accession codes CCDC 2118529 and 2118530 (compounds **16** and **30**) contain the supplementary crystallographic data for this paper. These data can be obtained free of charge via www.ccdc.cam.ac.uk/data_request/cif, or by emailing data_request@ccdc.cam.ac.uk, or by contacting The Cambridge Crystallographic Data Centre, 12 Union Road, Cambridge CB21EZ, UK; fax: +44 1223 336033.

Funding: The authors declare no competing financial interest. This work was financially supported by the Swiss Science National Foundation (SNF, Sinergia project CRSII5-173718 and project 310030_184662) (E.P., O.D., J.F., A.H., G.B., N.A.). The Synergy diffractometer was partially funded by the SNF within the R'Equip program (project 206021_177033).

Acknowledgments: Dr. Jürg Hauser and the X-ray crystal structure determination service unit, Department of Chemistry, Biochemistry and Pharmaceutical Sciences, University of Bern, are acknowledged for measuring, solving, refining, and summarizing the structures of BODIPY compounds **16** and **30**.

Conflicts of Interest: The authors declare no conflicts of interest.

*Corresponding authors:
Chemistry/Fluorescence studies:
Emilia Păunescu, paunescu_emilia@yahoo.com

Julien Furrer, Tel. +41-31-6844383, julien.furrer@unibe.ch
https://furrer.dcb.unibe.ch/
ORCID: 0000-0003-2096-0618

Parasitology, Fluorescence microscopy, TEM:
Andrew Hemphill, Tel. +41-31-6312384, Fax +41-31-6312477, andrew.hemphill@vetsuisse.unibe.ch
http://www.ipa.vetsuisse.unibe.ch/ueber_uns/personen/prof_dr_hemphill_andrew/index_ger.html
ORCID: 0000-0002-0622-2128

References

[1] aS. Thota, D. A. Rodrigues, D. C. Crans, E. J. Barreiro, *J. Med. Chem.* **2018**, *61*, 5805-5821; bS. M. Meier-Menches, C. Gerner, W. Berger, C. G. Hartinger, B. K. Keppler, *Chem. Soc. Rev.* **2018**, *47*, 909-928; cE. Alessio, L. Messori, *Molecules* **2019**, *24*.

[2] aJ. P. C. Coverdale, T. Laroiya-McCarron, I. Romero-Canelón, *Inorganics* **2019**, *7*, 31; bM. Adams, M. Hanif, C. G. Hartinger, in *Encyclopedia of Inorganic and Bioinorganic Chemistry*, John Wiley & Sons, Ltd. , **2017**, pp. 1-21; cG. Suss-Fink, *Dalton Trans.* **2010**, *39*, 1673-1688.

[3] aD. Gambino, L. Otero, *Inorg. Chim. Acta* **2012**, *393*, 103-114; bR. W. Brown, C. J. T. Hyland, *Med Chem. Comm.* **2015**, *6*, 1230-1243; cD. Gambino, L. Otero, *Inorg. Chim. Acta* **2018**, *472*, 58-75; dY. C. Ong, S. Roy, P. C. Andrews, G. Gasser, *Chem. Rev.* **2019**, *119*, 730-796; eF. Barna, K. Debache, C. A. Vock, T. Kuster, A. Hemphill, *Antimicrob. Agents Chemother.* **2013**, *57*, 5747-5754; fT. Kuster, N. Lense, F. Barna, A. Hemphill, M. K. Kindermann, J. W. Heinicke, C. A. Vock, *J. Med. Chem.* **2012**, *55*, 4178-4188; gB. Demoro, C. Sarniguet, R. Sanchez-Delgado, M. Rossi, D. Liebowitz, F. Caruso, C. Olea-Azar, V. Moreno, A. Medeiros, M. A. Comini, L. Otero, D. Gambino, *Dalton Trans.* **2012**, *41*, 1534-1543; hC. S. K. Rajapakse, A. Martinez, B. Naoulou, A. A. Jarzecki, L. Suarez, C. Deregnaucourt, V. Sinou, J. Schrevel, E. Musi, G. Ambrosini, G. K. Schwartz, R. A. Sanchez-Delgado, *Inorg. Chem.* **2009**, *48*, 1122-1131.

[4] aH. Yildirim, E. Guler, M. Yavuz, N. Ozturk, P. K. Yaman, E. Subasi, E. Sahin, S. Timur, *Mater. Sci. Eng. C* **2014**, *44*, 1-8; bA. Lapasam, L. Dkhar, N. Joshi, K. M. Poluri, M. R. Kollipara, *Inorg. Chim. Acta* **2019**, *484*, 255-263; cZ. Ude, I. Romero-Canelon, B. Twamley, D. F. Hughes, P. J. Sadler, C. J. Marmion, *J. Inorg. Biochem.* **2016**, *160*, 210-217; dQ. Laurent, L. K. Batchelor, P. J. Dyson, *Organometallics* **2018**, *37*, 915-923.

[5] J. Furrer, G. Süss-Fink, *Coord. Chem. Rev.* **2016**, *309*, 36-50.

[6] A. P. M. Basto, J.; Rubbiani, R.; Stibal, D.; Giannini, F.; Süss-Fink, G.; Balmer, V.; Hemphill, A.; Gasser, G.; Furrer, J. , *Antimicrob. Agents Chemother.* **2017**, *61*, e01031-01017.

[7] A. P. Basto, N. Anghel, R. Rubbiani, J. Muller, D. Stibal, F. Giannini, G. Suss-Fink, V. Balmer, G. Gasser, J. Furrer, A. Hemphill, *Metallomics* **2019**, *11*, 462-474.

[8] J. Jelk, V. Balmer, D. Stibal, F. Giannini, G. Suss-Fink, P. Butikofer, J. Furrer, A. Hemphill, *Exp. Parasitol.* **2019**, *205*, 107753.

[9] A. R. Timerbaev, *J. Anal. At. Spectrom.* **2021**, *36*, 254-266.

[10] B. Bertrand, K. Passador, C. Goze, F. Denat, E. Bodio, M. Salmain, *Coord. Chem. Rev.* **2018**, *358*, 108-124.

[11] aJ. C. Jagodinsky, A. Sulima, Y. Cao, J. E. Poprawski, B. N. Blackman, J. R. Lloyd, R. E. Swenson, M. M. Gottesman, M. D. Hall, *J. Biol. Inorg. Chem.* **2015**, *20*, 1081-1095; bM. K. Raza, S. Gautam, A. Garai, K. Mitra, P. Kondaiah, A. R. Chakravarty, *Inorg. Chem.* **2017**, *56*, 11019−11029; cS. Tasan, O. Zava, B. Bertrand, C. Bernhard, C. Goze, M. Picquet, P. Le Gendre, P. Harvey, F. Denat, A. Casini, E. Bodio, *Dalton Trans.* **2013**, *42*, 6102-6109; dR. P. Paitandi, V. Sharma, V. D. Singh, B. K. Dwivedi, S. M. Mobin, D. S. Pandey, *Dalton Trans.* **2018**, *47*, 17500-17514; eG. Gupta, A. Das, N. B. Ghate, T. Kim, J. Y. Ryu, J. Lee, N. Mandal, C. Y. Lee, *Chem. Commun.* **2016**, *52*, 4274-4277.

[12] A. A. Nazarov, J. Risse, W. H. Ang, F. Schmitt, O. Zava, A. Ruggi, M. Groessl, R. Scopelitti, L. Juillerat-Jeanneret, C. G. Hartinger, P. J. Dyson, *Inorg. Chem.* **2012**, *51*, 3633–3639.

[13] R. R. Kumara, R. Ramesha, J. G. Małeckib, *J. Organomet. Chem.* **2018**, *862*, 95-104.

[14] W. Ma, S. Zhang, Z. Tian, Z. Xu, Y. Zhang, X. Xia, X. Chen, Z. Liu, *Eur. J. Med. Chem.* **2019**, *181*, 111599.
[15] aJ. Z. Zhao, D.; Hua, W.; Li, W.; Xu, G.; Gou, S., *Organometallics* **2018**, *37*, 441−447; bL. Dondaine, D. Escudero, M. Ali, P. Richard, F. Denat, A. Bettaieb, P. Le Gendre, C. Paul, D. Jacquemin, C. Goze, E. Bodio, *Eur. J. Inorg. Chem.* **2016**, *2016*, 545-553.
[16] W. Ma, L. Guo, Z. Tian, S. Zhang, X. He, J. Li, Y. Yang, Z. Liu, *Dalton Trans.* **2019**, *48*, 4788-4793.
[17] P. D. Harvey, S. Tasan, C. P. Gros, C. H. Devillers, P. Richard, P. Le Gendre, E. Bodio, *Organometallics* **2015**, *34*, 1218–1227.
[18] aL. Yang, R. Simionescu, A. Lough, H. Yan, *Dyes Pigm.* **2011**, *91*, 264-267; bE. V. Rumyantsev, S. N. Alyoshin, Y. S. Marfin, *Inorg. Chim. Acta* **2013**, *408*, 181-185.
[19] aN. Boens, V. Leen, W. Dehaen, *Chem. Soc. Rev.* **2012**, *41*, 1130-1172; bM. S. Goncalves, *Chem. Rev.* **2009**, *109*, 190-212; cA. Loudet, K. Burgess, *Chem. Rev.* **2007**, *107*, 4891−4932.
[20] G. Ulrich, R. Ziessel, A. Harriman, *Angew. Chem., Int. Ed.* **2008**, *47*, 1184−1201.
[21] aR. Alford, H. Simpson, J. Duberman, G. C. Hill, M. Ogawa, C. Regino, H. Kobayashi, P. L. Choyke, *Mol. Imaging* **2009**, *8*, 341-354; bS. Zhang, T. Wu, J. Fan, Z. Li, N. Jiang, J. Wang, B. Dou, S. Sun, F. Song, X. Peng, *Org. Biomol. Chem.* **2013**, *11*, 555-558.
[22] T. Kowada, H. Maeda, K. Kikuchi, *Chem. Soc. Rev.* **2015**, *44*, 4953−4972.
[23] aA. V. Klein, T. W. Hambley, *Chem. Rev.* **2009**, *109*, 4911-4920; bH. Baruah, C. G. Barry, U. Bierbach, *Curr. Top. Med. Chem.* **2004**, *4*, 1537-1549.
[24] aM. A. Miller, B. Askevold, K. S. Yang, R. H. Kohler, R. Weissleder, *ChemMedChem* **2014**, *9*, 1131−1135; bM. K. Raza, S. Gautam, P. Howlader, A. Bhattacharyya, P. Kondaiah, A. R. Chakravarty, *Inorg. Chem.* **2018**, *57*, 14374-14385; cK. Mitra, S. Gautam, P. Kondaiah, A. R. Chakravarty, *ChemMedChem* **2016**, *11*, 1956-1967.
[25] aQ. X. Zhou, W. H. Lei, Y. J. Hou, Y. J. Chen, C. Li, B. W. Zhang, X. S. Wang, *Dalton Trans.* **2013**, *42*, 2786-2791; bB. Bertrand, P. E. Doulain, C. Goze, E. Bodio, *Dalton Trans.* **2016**, *45*, 13005-13011; cE. Bodio, P. Le Gendre, F. Denat, C. Goze, in *Insights from Imaging in Bioinorganic Chemistry, Vol. 68* (Eds.: R. van Eldik, C. D. Hubbard), Academic Press, **2016**, pp. 253-299.
[26] Z. Liu, I. Romero-Canelon, B. Qamar, J. M. Hearn, A. Habtemariam, N. P. Barry, A. M. Pizarro, G. J. Clarkson, P. J. Sadler, *Angew. Chem. Int. Ed.* **2014**, *53*, 3941-3946.
[27] A. Trommenschlager, F. Chotard, B. Bertrand, S. Amor, L. Dondaine, M. Picquet, P. Richard, A. Bettaïeb, P. Le Gendre, C. Paul, C. Goze, E. Bodio, *Dalton Trans.* **2017**, *46*, 8051-8056.
[28] O. Flores, A. Trommenschlager, S. Amor, F. Marques, F. Silva, L. Gano, F. Denat, M. P. Cabral Campello, C. Goze, E. Bodio, P. Le Gendre, *Dalton Trans.* **2017**, *46*, 14548-14555.
[29] A. Bhattacharyya, A. Dixit, S. Banerjee, B. Roy, A. Kumar, A. A. Karande, A. R. Chakravarty, *RSC Advances* **2016**, *6*, 104474-104482.
[30] T. Sun, X. Guan, M. Zheng, X. Jing, Z. Xie, *ACS Med. Chem. Lett.* **2015**, *6*, 430−433.
[31] aG. Ulrich, R. Ziessel, *J. Org. Chem.* **2004**, *69*, 2070-2083; bJ. Olmsted, *J. Phys. Chem.* **1979**, *83*, 2581–2584.
[32] G. Gupta, P. Kumari, J. Y. Ryu, J. Lee, S. M. Mobin, C. Y. Lee, *Inorg. Chem.* **2019**, *58*, 8587-8595.
[33] Y. Liu, Z. Li, L. Chen, Z. Xie, *Dyes Pigm.* **2017**, *141*, 5-12.
[34] T. J. Wang, Y. J. Hou, Y. J. Chen, K. Li, X. X. Cheng, Q. X. Zhou, X. S. Wang, *Dalton Trans.* **2015**, *44*, 12726-12734.
[35] J. M. Zimbron, K. Passador, B. Gatin-Fraudet, C.-M. Bachelet, D. Plażuk, L.-M. Chamoreau, C. Botuha, S. Thorimbert, M. Salmain, *Organometallics* **2017**, *36*, 3435−3442.
[36] R. P. Paitandi, S. Mukhopadhyay, R. S. Singh, V. Sharma, S. M. Mobin, D. S. Pandey, *Inorg. Chem.* **2017**, *56*, 12232-12247.
[37] A. Juris, V. Balzani, F. Barigelletti, S. Campagna, P. Belser, A. Von Zelewsky, *Coord. Chem. Rev.* **1988**, *84*, 85–277.
[38] M. Galletta, F. Puntoriero, S. Campagna, C. Chiorboli, M. Quesada, S. Goeb, R. Ziessel, *J. Phys. Chem. A* **2006**, *110*, 4348–4358.

[39] F. Giannini, M. Bartoloni, L. E. H. Paul, G. Süss-Fink, J.-L. Reymond, J. Furrer, *Med. Chem. Commun.* **2015**, *6*, 347-350
[40] D. Stibal, B. Therrien, G. Suss-Fink, P. Nowak-Sliwinska, P. J. Dyson, E. Cermakova, M. Rezacova, P. Tomsik, *J. Biol. Inorg. Chem.* **2016**, *21*, 443-452.
[41] O. Desiatkina, E. Paunescu, M. Mosching, N. Anghel, G. Boubaker, Y. Amdouni, A. Hemphill, J. Furrer, *ChemBioChem* **2020**, *21*, 2818-2835.
[42] O. Desiatkina, S. K. Johns, N. Anghel, G. Boubaker, A. Hemphill, J. Furrer, E. Păunescu, *Inorganics* **2021**, *9*, 59.
[43] O. Desiatkina, M. Mösching, N. Anghel, G. Boubaker, Y. Amdouni, A. Hemphill, J. Furrer, E. Păunescu, *Manuscript in preparation* **2022**.
[44] aC. E. Caffaro, J. C. Boothroyd, *Eukaryot. Cell* **2011**, *10*, 1095-1099; bA. J. Charron, L. D. Sibley, *J. Cell Sci.* **2002**, *115*, 3049-3059; cS. J. Nolan, J. D. Romano, I. Coppens, *PLoS Pathog.* **2017**, *13*, e1006362; dX. Hu, D. Binns, M. L. Reese, *J. Biol. Chem.* **2017**, *292*, 11009-11020; eA. F. Gomes, K. G. Magalhaes, R. M. Rodrigues, L. de Carvalho, R. Molinaro, P. T. Bozza, H. S. Barbosa, *Parasit Vectors* **2014**, *7*, 47.
[45] aE. Paunescu, G. Boubaker, O. Desiatkina, N. Anghel, Y. Amdouni, A. Hemphill, J. Furrer, *Eur. J. Med. Chem.* **2021**, *222*, 113610; bV. Studer, N. Anghel, O. Desiatkina, T. Felder, G. Boubaker, Y. Amdouni, J. Ramseier, M. Hungerbuhler, C. Kempf, J. T. Heverhagen, A. Hemphill, N. Ruprecht, J. Furrer, E. Paunescu, *Pharmaceuticals* **2020**, *13*, 471.
[46] M. A. Bennett, A. K. Smith, *J. Chem. Soc. Dalton Trans.* **1974**, 233-241.
[47] T. E. Wood, A. Thompson, *Chem. Rev.* **2007**, *107*, 1831-1861.
[48] aK. Krumova, G. Cosa, *J. Am. Chem. Soc.* **2010**, *132*, 17560-17569; bA. V. Omel'kov, Y. B. Pavlova, I. A. Boldyrev, J. G. Molotkovsky, *Russ. J. Bioorg. Chem.* **2007**, *33*, 505-510; cI. A. Boldyrev, J. G. Molotkovsky, *Russ. J. Bioorg. Chem.* **2006**, *32*, 78-83; dI. A. Boldyrev, X. H. Zhai, M. M. Momsen, H. L. Brockman, R. E. Brown, J. G. Molotkovsky, *J. Lipid Res.* **2007**, *48*, 1518-1532.
[49] aM. Ceulemans, K. Nuyts, W. M. De Borggraeve, T. N. Parac-Vogt, *Inorganics* **2015**, *3*, 516-533; bA. Sohail, K. Jayaraman, S. Venkatesan, K. Gotfryd, M. Daerr, U. Gether, C. J. Loland, K. T. Wanner, M. Freissmuth, H. H. Sitte, W. Sandtner, T. Stockner, *Plos Comput. Biol.* **2016**, *12*, e1005197.
[50] E. Paunescu, M. Soudani, C. M. Clavel, P. J. Dyson, *J. Inorg. Biochem.* **2017**, *175*, 198-207.
[51] S. Hanessian, J. A. Grzyb, F. Cengelli, L. Juillerat-Jeanneret, *Bioorg. Med. Chem.* **2008**, *16*, 2921-2931.
[52] aR. W. Wagner, J. S. Lindsey, *J. Am. Chem. Soc.* **1994**, *116*, 9759–9760; bC. Brückner, V. Karunaratne, S. Rettig, D. Dolphin, *Can. J. Chem.* **1996**, *74*, 2182-2193.
[53] A. Cui, X. Peng, J. Fan, X. Chen, Y. Wu, B. Guo, *J. Photochem. Photobiol. A* **2007**, *186*, 85–92.
[54] aA. A. Pakhomov, Y. N. Kononevich, A. A. Korlyukov, V. I. Martynov, A. M. Muzafarov, *Mendeleev Commun.* **2016**, *26*, 196-198; bW.-J. Shi, Y. Huang, W. Liu, D. Xu, S.-T. Chen, F. Liu, J. Hu, L. Zheng, K. Chen, *Dyes Pigm.* **2019**, *170*, 107566; cB. Matarranz, A. Sampedro, C. G. Daniliuc, G. Fernández, *Crystals* **2018**, *8*, 436; dY. S. Marfin, E. A. Banakova, D. A. Merkushev, S. D. Usoltsev, A. V. Churakov, *J. Fluoresc.* **2020**, *30*, 1611-1621.
[55] R. Reisfeld, R. Zusman, Y. Cohen, M. Eyal, *Chem. Phys. Lett.* **1988**, *147*, 142-147.
[56] J. Ramseier, D. Imhof, N. Anghel, K. Hanggeli, R. M. Beteck, V. Balmer, L. M. Ortega-Mora, R. Sanchez-Sanchez, I. Ferre, R. K. Haynes, A. Hemphill, *Molecules* **2021**, *26*.
[57] N. Anghel, J. Muller, M. Serricchio, J. Jelk, P. Butikofer, G. Boubaker, D. Imhof, J. Ramseier, O. Desiatkina, E. Paunescu, S. Braga-Lagache, M. Heller, J. Furrer, A. Hemphill, *Int J Mol Sci* **2021**, *22*.
[58] D. C. McFadden, F. Seeber, J. C. Boothroyd, *Antimicrob. Agents Chemother.* **1997**, *41* 1849-1853.
[59] J. Muller, A. Aguado-Martinez, V. Manser, V. Balmer, P. Winzer, D. Ritler, I. Hostettler, D. Arranz-Solis, L. Ortega-Mora, A. Hemphill, *Int. J. Parasitol. Drugs Drug. Resist.* **2015**, *5*, 16-25.

10.1002/cbic.202200536

Table of contents (ToC) entry:

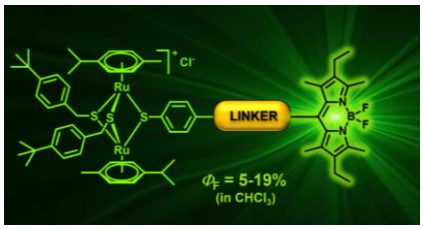

15 new dinuclear arene-ruthenium (II)-BODIPY conjugates were synthesized. Despite a fluorescence quenching effect, these conjugates can be used as fluorescent tracers. Their antiparasitic activity but also their toxicity against healthy HFFs are reduced compared to the parent ruthenium compounds. TEM images revealed profound alterations of the tachyzoite mitochondrion.